(A)

(B)

Fig. 4. Cytotoxicity of U0126 alone and cotreatment with imatinib in K562/W and K562/R cells. (A) K562/W (open triangles) and K562/R (closed triangles) cells were exposed to 0.0050 μM U0126 alone for 48 h. (B) K562/W (open symbols) and K562/R (closed symbols) cells were exposed to 0.0050–50 μM imatinib with (squares) or without (circles) 1 μM U0126 for 48 h. Cell viability was assayed by Alamar Blue. Each point represents the mean ± SD from six cells.
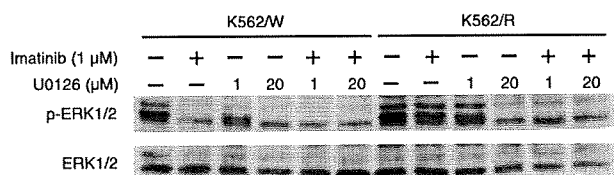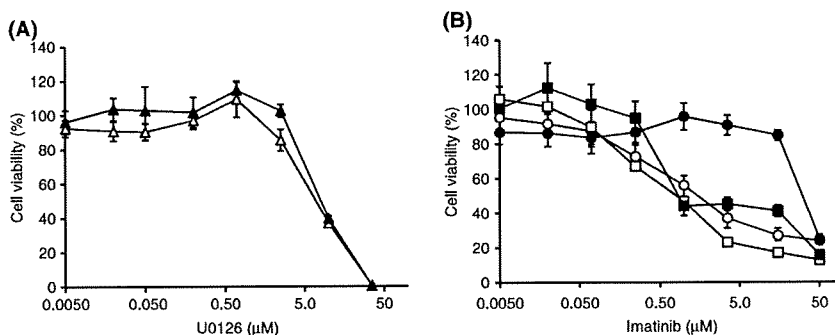

Fig. 5. The effects of imatinib and U0126, alone or in combination, on ERK1/2 phosphorylation. K562/W and K562/R cells were treated with or without 1 μM imatinib and U0126 (1 and 20 μM) for 24 h, as indicated.

cells, there was no difference in intracellular imatinib accumulation, which was not decreased by the P-gp inhibitor CysA (Fig. 1C,D). From these results, we hypothesized that P-gp functional activity was modulated by unknown factors in K562/R cells. Intracellular imatinib levels are possibly controlled by many factors, such as drug transporters and plasma carrier proteins, in vivo. Even though upregulation of MDR1 mRNA or protein is observed in imatinib-resistant CML patients, it will be necessary to measure intracellular imatinib levels to understand individual cases of imatinib resistance. Therefore, we ruled out a contribution from known mechanisms including P-gp, and postulated the involvement of a separate mechanism.

BCR–ABL has multiple downstream survival pathways, such as ERK1/2, ERK5, AKT, and JAK/STAT.[14–17] We examined whether imatinib treatment inhibited these downstream factors and found that the phosphorylation of BCR–ABL, ERK5, AKT, and STAT5 was indeed downregulated in both K562/W and K562/R cells, whereas ERK1/2 was not inhibited by imatinib in K562/R cells (Fig. 2A,C). A similar result was obtained by treatment using BCR–ABL siRNA (Fig. 3B), which further indicated that ERK1/2 is phosphorylated by a BCR–ABL-independent mechanism in the K562/R cells. Next, the contribution of ERK1/2 to imatinib resistance in the K562/R cells was examined (Figs 4,5). Although the cells were not sensitive to treatment with 1 μM imatinib alone, co-administration with 1 μM U0126 inhibited ERK1/2 phosphorylation and dramatically induced K562/R cell death. U0126 is a known inhibitor of ERK5 as well,[30] but because imatinib inhibited ERK5 phosphorylation (Fig. 2C), most of the synergistic effect of U0126 was presumably mediated by its downregulation of ERK1/2, rather than ERK5. These results demonstrate that inhibition of not only BCR–ABL, but also ERK1/2, due to its activation being independent of the former, is necessary to overcome imatinib resistance in the K562/R cells.

Concerning ERK1/2 activation in K562/R cells, the factors responsible have not been determined. It is known, however, that U0126 inhibits ERK1/2 through MEK1/2, which may be directly upstream of ERK1/2 in this BCR–ABL-independent pathway. We have also shown that the aberrant activation of LYN or KRAS is not involved (Fig. 1B; Supporting Information Fig. S1). However, the possibility remains that unknown factors

could increase ERK1/2 sensitivity and activate this signal via weak activation of BCR–ABL.

Recently, new drugs have been developed to target the BCR–ABL-dependent and -independent imatinib-resistance mechanisms. Nilotinib and dasatinib have a greater affinity for BCR–ABL than imatinib, and inhibit BCR–ABL and Src kinase, respectively.[31,32] U0126 co-treatment with dasatinib reverses LYN-dependent imatinib resistance,[33] suggesting the efficacy of its combination with molecular target drugs. Sorafenib, which inhibits multiple kinases, induces apoptosis in both BCR–ABL-expressing imatinib-sensitive and -resistant cells.[34–36] It is possible that the combination of sorafenib with a BCR–ABL inhibitor works by inhibiting ERK1/2 activation in K562/R cells.

In conclusion, we demonstrate that ERK1/2, activated through a BCR–ABL-independent mechanism, contributes to imatinib resistance in certain CML cells (Supporting Information Fig. S3). Although further work is required to confirm whether or not this resistance mechanism occurs in patients with CML, our study shows that this mechanism can be overcome by inhibiting the ERK1/2 signaling pathway with specific drugs that could be candidates for targeting the CML cells resistant to imatinib.

Acknowledgments

Disclosure Statement

None.

Abbreviations

ABL	Abelson
AKT	v-akt murine thymoma viral oncogene homolog
BCL	B-cell CLL/lymphoma 2
BCR	breakpoint cluster region
CML	chronic myeloid leukemia
CysA	cyclosporin A
LYN	v-yes-1 Yamaguchi sarcoma viral related oncogene homolog
P-gp	P-glycoprotein
PI3K	phosphoinositide 3-kinase
RAF	v-raf murine sarcoma viral oncogene homolog
RAS	rat sarcoma oncogene
STAT	signal transducer and activator of transcription

Nambu *et al.*

References

1 Kalidas M, Kantarjian H, Talpaz M. Chronic myelogenous leukemia. *JAMA* 2001; **286**: 895–8.
2 Capdeville R, Buchdunger E, Zimmermann J, Matter A. Glivec (STI571, imatinib), a rationally developed, targeted anticancer drug. *Nat Rev Drug Discov* 2002; **1**: 493–502.
3 Druker BJ, Guilhot F, O'Brien SG *et al.* Five-year follow-up of patients receiving imatinib for chronic myeloid leukemia. *N Engl J Med* 2006; **355**: 2408–17.
4 Daley GQ. Dodging the magic bullet: understanding imatinib resistance. *Cancer Biol Ther* 2003; **2**: 109–10.
5 Branford S, Rudzki Z, Walsh S *et al.* High frequency of point mutations clustered within the adenosine triphosphate-binding region of BCR/ABL in patients with chronic myeloid leukemia or Ph-positive acute lymphoblastic leukemia who develop imatinib (STI571) resistance. *Blood* 2002; **99**: 3472–5.
6 Roche-Lestienne C, Soenen-Cornu V, Grardel-Duflos N *et al.* Several types of mutations of the Abl gene can be found in chronic myeloid leukemia patients resistant to STI571, and they can pre-exist to the onset of treatment. *Blood* 2002; **100**: 1014–8.
7 Gorre ME, Mohammed M, Ellwood K *et al.* Clinical resistance to STI-571 cancer therapy caused by BCR–ABL gene mutation or amplification. *Science* 2001; **293**: 876–80.
8 Hamada A, Miyano H, Watanabe H, Saito H. Interaction of imatinib mesilate with human P-glycoprotein. *J Pharmacol Exp Ther* 2003; **307**: 824–8.
9 Hirayama C, Watanabe H, Nakashima R *et al.* Constitutive overexpression of P-glycoprotein, rather than breast cancer resistance protein or organic cation transporter 1, contributes to acquisition of imatinib-resistance in K562 cells. *Pharm Res* 2008; **25**: 827–35.
10 Mahon FX, Belloc F, Lagarde V *et al.* MDR1 gene overexpression confers resistance to imatinib mesylate in leukemia cell line models. *Blood* 2003; **101**: 2368–73.
11 Gambacorti-Passerini C, Barni R, le Coutre P *et al.* Role of alpha1 acid glycoprotein in the *in vivo* resistance of human BCR–ABL(+) leukemic cells to the abl inhibitor STI571. *J Natl Cancer Inst* 2000; **92**: 1641–50.
12 Donato NJ, Wu JY, Stapley J *et al.* BCR–ABL independence and LYN kinase overexpression in chronic myelogenous leukemia cells selected for resistance to STI571. *Blood* 2003; **101**: 690–8.
13 Dai Y, Rahmani M, Corey SJ, Dent P, Grant S. A Bcr/Abl-independent, Lyn-dependent form of imatinib mesylate (STI-571) resistance is associated with altered expression of Bcl-2. *J Biol Chem* 2004; **279**: 34227–39.
14 Jin A, Kurosu T, Tsuji K *et al.* BCR/ABL and IL-3 activate Rap1 to stimulate the B-Raf/MEK/Erk and Akt signaling pathways and to regulate proliferation, apoptosis, and adhesion. *Oncogene* 2006; **25**: 4332–40.
15 Sonoyama J, Matsumura I, Ezoe S *et al.* Functional cooperation among Ras, STAT5, and phosphatidylinositol 3-kinase is required for full oncogenic activities of BCR/ABL in K562 cells. *J Biol Chem* 2002; **277**: 8076–82.
16 Kirchner D, Duyster J, Ottmann O, Schmid RM, Bergmann L, Munzert G. Mechanisms of BCR–ABL-mediated NF-kappaB/Rel activation. *Exp Hematol* 2003; **31**: 504–11.
17 Buschbeck M, Hofbauer S, Di Croce L, Keri G, Ullrich A. Abl-kinase-sensitive levels of ERK5 and its intrinsic basal activity contribute to leukaemia cell survival. *EMBO Rep* 2005; **6**: 63–9.
18 Quintas-Cardama A, Cortes J. Molecular biology of BCR–ABL1-positive chronic myeloid leukemia. *Blood* 2009; **113**: 1619–30.
19 Pendergast AM, Quilliam LA, Cripe LD *et al.* BCR–ABL-induced oncogenesis is mediated by direct interaction with the SH2 domain of the GRB-2 adaptor protein. *Cell* 1993; **75**: 175–85.
20 McCubrey JA, Steelman LS, Abrams SL *et al.* Roles of the RAF/MEK/ERK and PI3K/PTEN/AKT pathways in malignant transformation and drug resistance. *Adv Enzyme Regul* 2006; **46**: 249–79.
21 Nishimoto S, Nishida E. MAPK signalling: ERK5 versus ERK1/2. *EMBO Rep* 2006; **7**: 782–6.
22 O'Brien J, Wilson I, Orton T, Pognan F. Investigation of the Alamar Blue (resazurin) fluorescent dye for the assessment of mammalian cell cytotoxicity. *Eur J Biochem* 2000; **267**: 5421–6.
23 Brauer KM, Werth D, von Schwarzenberg K *et al.* BCR–ABL activity is critical for the immunogenicity of chronic myelogenous leukemia cells. *Cancer Res* 2007; **67**: 5489–97.
24 Pao W, Wang TY, Riely GJ *et al.* KRAS mutations and primary resistance of lung adenocarcinomas to gefitinib or erlotinib. *PLoS Med* 2005; **2**: e17.
25 Agarwal A, Eide CA, Harlow A *et al.* An activating KRAS mutation in imatinib-resistant chronic myeloid leukemia. *Leukemia* 2008; **22**: 2269–72.
26 Bain J, McLauchlan H, Elliott M, Cohen P. The specificities of protein kinase inhibitors: an update. *Biochem J* 2003; **371**: 199–204.
27 Garnett MJ, Marais R. Guilty as charged: B-RAF is a human oncogene. *Cancer Cell* 2004; **6**: 313–9.
28 Weinstein-Oppenheimer CR, Henriquez-Roldan CF, Davis JM *et al.* Role of the Raf signal transduction cascade in the *in vitro* resistance to the anticancer drug doxorubicin. *Clin Cancer Res* 2001; **7**: 2898–907.
29 Davis JM, Navolanic PM, Weinstein-Oppenheimer CR *et al.* Raf-1 and Bcl-2 induce distinct and common pathways that contribute to breast cancer drug resistance. *Clin Cancer Res* 2003; **9**: 1161–70.
30 Kamakura S, Moriguchi T, Nishida E. Activation of the protein kinase ERK5/BMK1 by receptor tyrosine kinases. Identification and characterization of a signaling pathway to the nucleus. *J Biol Chem* 1999; **274**: 26563–71.
31 Kantarjian H, Giles F, Wunderle L *et al.* Nilotinib in imatinib-resistant CML and Philadelphia chromosome-positive ALL. *N Engl J Med* 2006; **354**: 2542–51.
32 Talpaz M, Shah NP, Kantarjian H *et al.* Dasatinib in imatinib-resistant Philadelphia chromosome-positive leukemias. *N Engl J Med* 2006; **354**: 2531–41.
33 Nguyen TK, Rahmani M, Harada H, Dent P, Grant S. MEK1/2 inhibitors sensitize Bcr/Abl+ human leukemia cells to the dual Abl/Src inhibitor BMS-354/825. *Blood* 2007; **109**: 4006–15.
34 Wilhelm SM, Carter C, Tang L *et al.* BAY 43-9006 exhibits broad spectrum oral antitumor activity and targets the RAF/MEK/ERK pathway and receptor tyrosine kinases involved in tumor progression and angiogenesis. *Cancer Res* 2004; **64**: 7099–109.
35 Rahmani M, Nguyen TK, Dent P, Grant S. The multikinase inhibitor sorafenib induces apoptosis in highly imatinib mesylate-resistant bcr/abl+ human leukemia cells in association with signal transducer and activator of transcription 5 inhibition and myeloid cell leukemia-1 down-regulation. *Mol Pharmacol* 2007; **72**: 788–95.
36 Kurosu T, Ohki M, Wu N, Kagechika H, Miura O. Sorafenib induces apoptosis specifically in cells expressing BCR/ABL by inhibiting its kinase activity to activate the intrinsic mitochondrial pathway. *Cancer Res* 2009; **69**: 3927–36.

Supporting Information

Additional Supporting Information may be found in the online version of this article:

Fig. S1. Mutation analysis of KRAS in (A) K562/W and (B) K562/R cells. The T519C silent mutation was observed in both cell lines.

Fig. S2. (A) Expression of P-glycoprotein in crude membrane fractions of K562/W, K562/R, and prevK562/R cells. (B) Effects of imatinib treatment on the phosphorylation levels of ERK1/2 in K562/W, K562/R, and prevK562/R cells. Cells were treated with the indicated concentrations of imatinib for 24 h, and phosphorylation levels were analyzed by Western blotting.

Fig. S3. Scheme of a BCR–ABL-independent imatinib-resistant mechanism in K562/R cells. In K562/R cells, ERK1/2 is activated by a BCR–ABL-independent pathway. Imatinib inhibits BCR–ABL and decreases phosphorylated AKT, but not phosphorylated ERK1/2, which is activated by an unknown protein independent of BCR–ABL.

Please note: Wiley-Blackwell are not responsible for the content or functionality of any supporting materials supplied by the authors. Any queries (other than missing material) should be directed to the corresponding author for the article.

Suppression of galectin-3 expression enhances apoptosis and chemosensitivity in liver fluke-associated cholangiocarcinoma

Sopit Wongkham,[1,4,6] Mutita Junking,[1,4] Chaisiri Wongkham,[1,4] Banchob Sripa,[2,4] Siri Chur-in[3,4] and Norie Araki[5,6]

Departments of [1]Biochemistry, [2]Pathology, [3]Surgery, [4]Liver Fluke and Cholangiocarcinoma Research Center, Faculty of Medicine, Khon Kaen University, Khon Kaen, Thailand; [5]Department of Tumor Genetics and Biology, Graduate School of Medical Sciences, Kumamoto University, Kumamoto, Japan

Cholangiocarcinoma (CCA) is a fatal disease with high resistance to anticancer drugs. This is probably in part due to enhanced resistance to apoptosis. We have previously shown that galectin-3 (Gal-3), a β-galactoside-binding lectin, is highly expressed in CCA tissues. In this study, we demonstrated further that Gal-3 plays a direct role in anti-apoptosis regardless of the apoptotic insults. The anti-apoptotic activity and chemoresistance of CCA cells were related to Gal-3 expression level. Suppression of Gal-3 expression with siRNA stimulated apoptosis. siGal-3-K626 transiently depleted Gal-3 expression to the baseline and dramatically induced apoptosis, while siGal-3-K402 suppressed Gal-3 expression by 50% and provoked cell apoptosis, but only under apoptotic insults (hypoxic conditions or short UV radiation). These actions were reversed in Gal-3 overexpressing CCA cells. The correlation between the degree of anti-apoptotic activity and the level of endogenous Gal-3 was demonstrated. Suppression of Gal-3 expression in CCA cells with siGal-3-K402 significantly enhanced apoptosis induced by cisplatin or 5-fluorouracil by approximately 10 times, whereas overexpression of Gal-3 led to an increased resistance to drugs. In summary, the present study showed that the cellular level of Gal-3 might contribute to the anti-apoptotic activity and chemoresistance of CCA cells. Hence, Gal-3 expression level in cancer cells or tissues may be a marker for predicting chemotherapeutic response, and Gal-3 may be a specific gene-targeting therapy option for treating CCA. (*Cancer Sci* 2009; 100: 2077–2084)

C holangiocarcinoma (CCA), bile duct cancer, occurs with a varying frequency in different geographic regions of the world. It is rare in Western countries; however, in Khon Kaen, a province in the north-east of Thailand, the incidences of CCA in male and female residents are highest in the world.[1] The risk factor for CCA in this region has been shown to be the infection of liver fluke, *Opisthorchis viverrini*,[2] whereas primary sclerosing cholangitis, hepatolithiasis, and choledochal cysts are risk factors for CCA in Western countries.

Cholangiocarcinoma (CCA) has traditionally resulted in a high mortality rate and poor prognosis. Although surgery is potentially curative in certain patients, failure has usually occurred due to recurrence. Adjuvant or neo-adjuvant therapy by chemotherapeutic drugs has been shown to improve local control, provide palliation, and prolong survival in various cancers; however, this is uncommon for CCA, owing to its poor response to therapy.[3] Currently, adjuvant therapy, which enhances the cytotoxicity of chemotherapeutic drugs or sensitizes tumor cells to anticancer drugs, is showing encouraging results. This approach may increase the effectiveness of chemotherapy and improve prognosis in patients with CCA.

Recently, we have reported that all 53 CCA tissues expressed galectin 3 (Gal-3) regardless of histological type. A lower intensity was found in poorly differentiated CCA and was related to

lymphatic invasion.[4] Even though there is substantial evidence regarding Gal-3 expression in various cancers, the significance of Gal-3 in the carcinogenesis and progression of CCA is yet to be determined.

Galectins are a family of proteins characterized by their affinity for β-galactoside, and the sequence similarities in the carbohydrate-recognition domain.[5] To date, at least 15 galectin members have been identified and classified according to their structures into proto, chimera, and tandem-repeat types.[6] Galectin-3 (Gal-3), a multifunctional protein, participates in a variety of biological events, for example cell adhesion, differentiation, proliferation, and apoptosis.[5,7,8] Gal-3 has recently been shown to play a role in anti-apoptosis in several cell types.[9–13] Peritoneal macrophages from Gal-3-deficient mice were more sensitive to apoptotic stimuli than those from control mice.[14] Gal-3 could inhibit epithelial cell apoptosis induced by staurosporine, cisplatin, genistein, and anoikis.[9–11,13] In addition, transfecting Gal-3 into epithelial cells provided them with resistance to apoptotic insult.[9–13]

In this study, we examined the role of Gal-3 in anti-apoptosis in CCA cell lines by using RNA interference (RNAi) to knockdown endogenous Gal-3 expression. The possibility of using RNAi-mediated knockdown of Gal-3, in combination with a chemotherapeutic agent, is explored as a more effective treatment for CCA.

Materials and Methods

Cell culture. Four CCA cell lines were established from different histological grading of primary CCA tumors, KKU-OCA17 from a well-differentiated type, KKU-M055 and KKU-M214 from moderately differentiated types, and KKU-100 from a poorly differentiated type, as described by Sripa, *et al.*[15] CCA cells were cultured in Ham's F-12 (Life Technologies, Rockville, MD, USA) supplemented with 10% fetal calf serum, 100 U/mL penicillin, and 100 μg/mL streptomycin at 37°C and 5% CO_2.

Short interference RNA transfection. The coding sequence of the *Gal-3* gene in the human genome was submitted to Ambion siRNA Target Finder (http://www.ambion.com/techlib/misc/siRNA_finder.html). Two siRNAs specific for human galectin-3, siGal-3-K402 and siGal-3-K626, derived from the mRNA sequences beginning at nt 402 (5′-GGTGCCTCGCATGCTGA-TAAC-3′) and nt 626 (5′-AAGTACTGGTTGAACCTGACC-3′), respectively, were purchased from JbioS (JbioS, Saitama, Japan). The lyophilized siRNAs were dissolved in annealing buffer, reheated to 95°C for 1 min, and incubated for 1 h at 37°C, by the protocol described previously.[16] Transfection of both sequences was performed using Lipofectamine 2000

(Invitrogen, Carlsbad, CA, USA) according to the manufacturer's instructions. CCA cells (8×10^4 cells in 2 mL complete culture medium) were seeded into a six-well plate for 24 h before transfection. The double-stranded siRNAs (100 pM) were transiently transfected into CCA cell lines KKU-100 and KKU-M214 using (2 µg) Lipofectamine 2000 according to the manufacturer's instructions. After 4 h, the medium was changed to complete culture medium (Ham's F-12 with 10% fetal calf serum), and siRNA treated cells were used in the *in vitro* study within 48–72 h after transfection. As a control, cells were treated with siRNA-scramble (Ambion, Austin, TX, USA) or Lipofectamine 2000 under identical conditions.

Western blot analysis. Endogenous Gal-3 levels were determined using Western blotting. Before cell lysate preparation, apoptotic cells were washed out with PBS and then the adhered cells were extracted with lysis buffer (8 M Urea, 4% CHAPS) containing a complete protease inhibitor cocktail (Roche Molecular Biochemicals, Mannheim, Germany). The lysate was subjected to 12.5% SDS–polyacrylamide gel electrophoresis,[17] and the protein expression of Gal-3 in CCA cells was determined by immunoblotting.[18] Gal-3 was detected by 1:10 000 anti-Gal-3 antibody (Chemicon, Temecula, CA, USA), or 1:5000 anti-β-actin antibody (Sigma-Aldrich, St. Louis, MO, USA) as an internal control. The membrane was probed with horseradish peroxidase–conjugated antibody at 1:10 000 dilution (GE Healthcare, Buckinghamshire, UK). The immunoreactive proteins were visualized by Western Lightning Chemiluminescence Reagents (PerkinElmer, Boston, MA, USA). Quantitative analysis of Gal-3/β-actin expression was performed using the Gel-Pro analyzer (Media Cybernetics, Silver Spring, MD, USA).

Time lapse assay. After 4 h of siRNA transfection, cells cultured in complete medium were placed under a time-lapse microscope and cultured further for 72 h, at 37°C and 5% CO_2. The images were obtained using an ×20 UPlan Apo objective (Olympus, Tokyo, Japan). The camera, shutters, and filter wheel were controlled by MetaMorph imaging software (Universal Imaging, Dawningtown, PA, USA), and the images were collected at 5-min intervals for 48 h. Analysis was performed using MetaMorph software (Universal Imaging).

Construction of GFP Gal-3 expression vector. Human Gal3-inserted pET vector (Novagen, Madison, WI, USA) was a gift from Dr Ryuji Nagai (Department of Biochemistry, Kumamoto University School of Medicine, Kumamoto, Japan). DNA coding for Gal-3 was cut from the vector at the *Eco*RI site, followed by insertion into the multiple cloning site of the vector pEGFP-C1 (Clontech, Mountain View, CA, USA). The orientation of the construct was confirmed by digestion with *Sma*I, and the DNA sequence of the insertion was confirmed with a DNA sequencer (Applied Biosystems, Framingham, MA, USA). The plasmid was then transfected into KKU-M055 using Lipofectamine 2000 according to the manufacturer's instructions. After 24 h, the medium was changed to Medium G (Ham's F-12 medium containing 10% fetal calf serum and 0.6 mg/mL of G418 [Gibco, Carlsbad, CA, USA]). The cells were cultured in medium G for 2 weeks, and colonies resistant to G418 were screened by immunoblotting using the anti-Gal-3 antibody (Chemicon). Cells transfected with pEGFP-C1 vector without Gal-3 cDNA were used as a control.

Cell proliferation assay and drug treatment. After 24 h of siRNA transfection, cells were treated with various concentrations of cisplatin and 5-fluorouracil (5-FU) then incubated at 37°C, 5% CO_2 for another 48 h. The number of cells was determined using a sulforhodamine B assay (SRB; Sigma-Aldrich).[19] Briefly, the culture medium was removed, and 10% cold trichloroacetic acid was added for 1 h at 4°C, and subsequently washed five times with deionized water. The plates were then air-dried and 0.4% SRB in 1% acetic acid was added for

30 min. Unbound dye was washed out five times with 1% acetic acid. After air-drying, SRB dye within cells were solubilized with 200 µL of 10 mM Tris-base solution, and plates were shaken for at least 5 min. Absorbance was measured at 540 nm using a microplate reader (Tecan Austria, Salburg, Austria).

Hypoxic conditions and UV irradiation. After 24 h of siRNA transfection, the cells were grown further at 37°C under hypoxic conditions (5% CO_2, 10% H_2, and 85% N_2) for 48 h, or exposed directly to UV radiation (250 mJoule/m^2) for 4 s and then incubated at 37°C, 5% CO_2 for 48 h. The number of cells was determined using the sulforhodamine B assay.

Immunocytofluorescence staining. Cells were fixed in 4% paraformaldehyde for 15 min, permeabilized with 0.2% Triton X-100 for 5 min, and blocked with 1% bovine serum albumin in PBS for 1 h. Then, cells were incubated in 1:8000 of mouse monoclonal anti-Gal-3 antibody (Chemicon) for 1 h, then 1:1000 FITC goat antimouse IgG (BioSource, Camarillo, CA, USA) and 1:200 Hoechst 33342 (Molecular Probes, Eugene, OR, USA) for 1 h. The stained cells were observed using immunofluorescent microscope (Olympus).

Detection of apoptotic cells by flow cytometry using annexin V assay. After 24 h of siRNA transfection, cells were gently trypsinized and washed with ice-cold PBS. The cell pellet was resuspended in 100 µL of Annexin-V-FLUOS labeling solution (Roche, Penzberg, Germany) and incubated at room temperature for 15 min. At least 20 000 cells were counted by flow cytometry (FACSCalibur flow cytometer) and data were analyzed using Cell Quest software (Becton Dickinson, San Jose, CA, USA).

Statistical analysis. Statistical analyses were performed using Sigma Stat version 3.1 software (Systat Software UK, London, UK). Results from flow cytometry, drug treatment, hypoxic condition, and UV irradiation are presented as mean ± SD, and the significance of the differences were addressed by Student's *t*-test. A *P*-value of <0.05 was considered statistically significant.

Results

Suppression of Gal-3 induced apoptosis. To address the functional importance of Gal-3, we employed RNAi to transiently deplete the expression of Gal-3 in two CCA cell lines, KKU-100 and KKU-M214, which had high expression levels of Gal-3. Two siRNAs of 21-mer oligoribonucleotides targeting Gal-3, siGal-3-K402 and siGal-3-K626, were designed to suppress Gal-3 expression. The efficiency of the siGal-3s in suppression of endogenous Gal-3 is shown in Figure 1. As shown by Western blot analysis, transfection of KKU-100 CCA cells with siGal-3-K626 dramatically reduced Gal-3 protein >90% within 24 h, whereas cells transfected with siGal-3-K402 showed partial suppression of Gal-3 expression (~50%) (Fig. 1A). The efficiency of the siRNA was observed as early as 6 h after siGal-3 transfection and before apoptotic effect was observed (Fig. S1). Moreover, siGal-3 treatment effectively suppressed the level of Gal-3 in a time-dependent manner, and the suppression effects were detected until 72 h after transfection (Fig. 1B). Similar results were observed for KKU-M214 cells (data not shown). Neither siRNA-scramble, nor Lipofectamine 2000, affected the level of Gal-3 expression.

Within 24 h of siGal-3treatment, apoptotic nuclei were readily observed in the cells treated with siGal-3-K626, but not in those treated with siGal-3-K402 or in control cells treated with Lipofectamine 2000 (Fig. 2A). To determine the anti-apoptotic activity of Gal-3, KKU-100 CCA cells transfected with siGal-3-K626 for 24 h were analyzed by flow cytometry using Annexin V and propidium iodide staining for early and late apoptotic cells. As shown in Figure 2(B), the number of Annexin V positive cells was much higher in KKU-100 cells treated with siGal-3-K626 compared to the control. Gal-3 suppressed
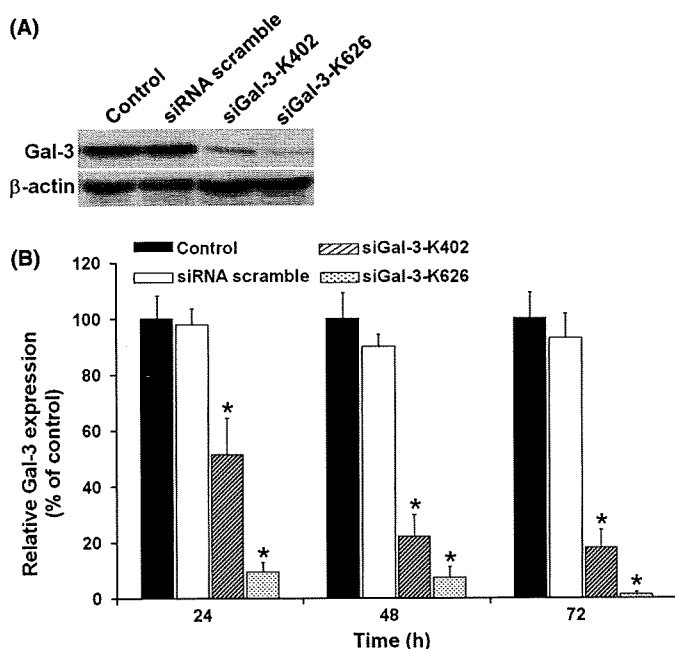
(A)

Gal-3

β-actin

(B)

Fig. 1. Galectin-3 (Gal-3) suppression by siGal-3. Cholangiocarcinoma (CCA) cell line KKU-100 cells were transfected with siGal-3-K626 or siGal-3-K402 or siRNA-scramble using Lipofectamine 2000. (A) Expression of Gal-3 protein by immunoblotting with anti-Gal-3 after siGal-3 transfection for 72 h. (B) Relative Gal-3 expression levels (% of control) after siGal-3 transfection for 24 h, 48 h, and 72 h. Results are the mean ± SE (bars) of three independent experiments. *$P < 0.05$ compared with control cells.

cells underwent 70% apoptotic cell death, whereas only 5% of apoptotic cells were detected in the Gal-3 expressing cells ($P < 0.05$) (Fig. 2C).

Suppression of Gal-3 enhanced hypoxia and UV induced apoptosis. To demonstrate the anti-apoptotic role of Gal-3, CCA cell lines KKU-100 and KKU-M214, with or without transfection of siGal-3-K402, were induced to apoptosis by hypoxic conditions or UV irradiation. Compared to the parental

control and siRNA-scramble-treated cells, the exposure of siGal-3-K402-treated cells to hypoxic conditions for 48 h resulted in significantly more apoptotic cells: 82.1 ± 0.58% and 65.5 ± 1.2% for KKU-100 and KKU-M214, respectively ($P < 0.05$) (Fig. 3A). Similarly, a short UV irradiation induced apoptosis in siGal-3-treated cells more than it did in the controls ($P < 0.05$). Exposure of CCA cells to UV caused an increase of 29.4 ± 2.6% and 13.9 ± 1.2% in apoptotic cells in siGal-3-K402-treated KKU-100 and KKU-M214, respectively (Fig. 3B). These results suggest a common role for Gal-3 in the anti-apoptotic process, regardless of the apoptotic inducer.

To investigate whether constitutive Gal-3 expression in CCA cells affected resistance to apoptotic stress, the anti-apoptotic activity of three CCA cell lines with different levels of Gal-3 expression, KKU-100 (high), KKU-OCA17 (moderate), and KKU-M055 (low), were examined under hypoxic conditions or UV irradiation. As shown in Figure 3(C), when comparing the corresponding control cells without apoptotic induction, the exposure of CCA cells to hypoxic conditions resulted in apoptosis of 74.3 ± 1.4% in KKU-100, 85.3 ± 0.8% in OCA17, and 89.9 ± 0.8% in KKU-M055. Similarly, the exposure of CCA cells to UV radiation induced apoptosis of 46.2 ± 5.2% in KKU-100, 88.9 ± 3.9% in OCA17, and 73.4 ± 2.5% in KKU-M055. These data reveal an important role of Gal-3 in regulating cell responses to apoptotic insults. The anti-apoptotic activity corresponded to the level of endogenous Gal-3 expression: the higher the level of endogenous Gal-3 expression, the higher the anti-apoptotic activity.

To ensure that UV irradiation did not alter Gal-3 expression, endogenous Gal-3 protein levels in KKU-100, KKU-OCA17, and KKU-M055 cells were determined 48 h after UV exposure. As shown in Figure 3(D), the levels of Gal-3 expression in all cell lines were not varied after UV irradiation; hence the anti-apoptotic response was based on the endogenous Gal-3.

Overexpression of Gal-3 rescued cells from apoptosis. To reveal the contribution of Gal-3 to anti-apoptosis, we next constructed an overexpressed Gal-3 CCA cell line using GFP expression vector pEGFP-C1-hGal3. KKU-M055, which had a low level of endogenous Gal-3, was transfected with pEGFP-C1-hGal3 or the control vector (pEGFP-C1), as controls. GFP-expressing cells observed by phase-contrast and fluorescence microscopy are shown in Figure 4(Aa,b). Transfection of
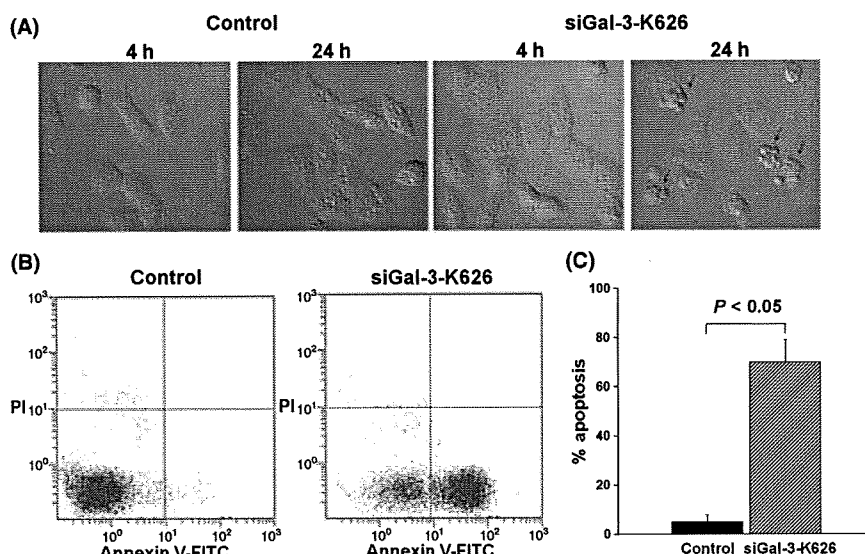
(A) Control   siGal-3-K626

(B)

(C)

Fig. 2. Induction of apoptosis in cholangiocarcinoma (CCA) cell lines treated with siGal-3-K626. (A) Cell morphology of control and siGal-3-K626-treated cells was observed by time-lapse microscopy at 4 h and 24 h after transfection. (B) Apoptotic cells were detected in siGal-3-K626-treated cells using Annexin V and PI (propidium iodide) staining followed by flow cytometry. (C) The percentages of apoptotic cells were compared between siGal-3-K626-treated cells and controls. Results are the mean ± SE of three independent experiments.
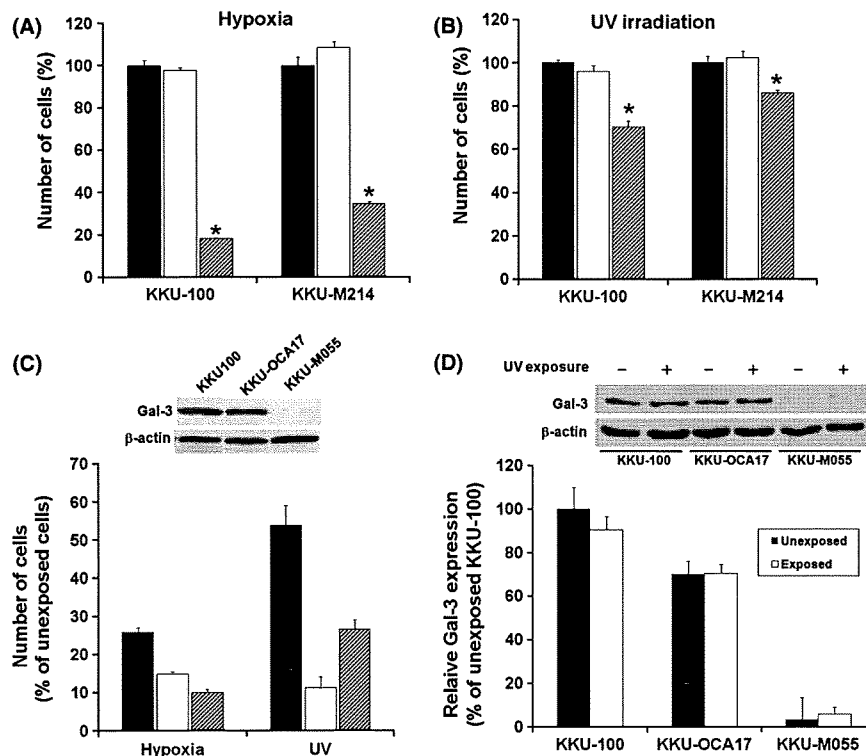
Wongkham *et al.*

Fig. 3. siGal-3-K402 enhanced apoptosis in cholangiocarcinoma (CCA) cells under hypoxia and UV-induced apoptosis. CCA cell lines KKU-100 or KKU-M214 were treated with siRNA-scramble or siGal-3-K402 for 24 h, then grown (A) under hypoxic conditions for 48 h or (B) briefly exposed to UV radiation, then incubated at 37°C and 5% CO_2 for 48 h. The cell numbers were determined by sulforhodamine-B (SRB) assay thereafter: siGal-3-K402-treated cells (slash bar), parental cells (black bar), and siRNA-scramble cells (white bar). (C) Effects of hypoxia and UV-induced apoptosis on CCA cell lines with different endogenous galectin-3 (Gal-3) expressions: KKU-100 (high expression, black bar), KKU-OCA17 (moderate expression, white bar), and KKU-M055 (low expression, slash bar). (D) Endogenous Gal-3 expression of CCA cell lines after a short UV irradiation and culture for a further 48 h. Expressions of Gal-3 in KKU-100, KKU-OCA17, and KKU-M055 were determined by immunobloting (upper inset) and relative Gal-3 expression level (% of unexposed KKU-100) between UV-unexposed cells (black bar) and UV-exposed cells (white bar) were compared. Results are the mean ± SE of three independent experiments. *$P < 0.05$.

KKU-M055 cells with pEGFP-C1-hGal3 GFP vector resulted in 50–60% of GFP-labeled cells. The efficiency of transfection was monitored via GFP expressing cells. Approximately 50–60% of KKU-M055 cells were transfected with pEGFP-C1-hGal3. Moreover, cytofluorescence staining indicated that GFP-Gal-3 expressed in pEGFP-C1-hGal3-transfected cells could function in a similar manner to endogenous Gal-3 observed in KKU-100 cells. GFP-Gal-3 was found predominantly in the nucleus (Fig. 4Ac,d,g–h), and it translocated from the nucleus to the cytoplasm under apoptotic insult (Fig. 4Ai,j), as it did in KKU-100 cells (Fig. 4 Ae,f). The overexpression of Gal-3 protein was confirmed by Western blot analysis (Fig. 4B). Gal-3 expression in these cells was approximately 2.5-fold higher than the parental cells or pEGFP-C1-treated cells (Fig. 4C).

The anti-apoptotic role of Gal-3 in pEGFP-C1-hGal-3-transfected cells was compared with the parental (KKU-M055) cells and the control pEGFP-C1 vector–transfected cells, by culturing cells in hypoxic conditions or short term exposure to UV irradiation. As shown in Figure 4(E), hypoxic conditions or short UV exposure dramatically induced cell apoptosis of parental and control cells to <20% and 25% of the unexposed cells, respectively. Resistance to these apoptotic insults, however, was demonstrated in the Gal-3 overexpressing KKU-M055 cells. The numbers of pEGFP-C1-hGal3-transfected cells that remained in both apoptotic-induced conditions were significantly higher than those of the control cells ($P < 0.05$) (Fig. 4E).

Suppression of Gal-3 expression enhanced anticancer drug-induced apoptosis. To determine whether drug-induced apopto-

sis was enhanced by suppression of Gal-3 expression in CCA cell lines, siGal-3-K402 treated cells were cultured in the absence or presence of an anticancer drug for 48 h, and cell numbers were determined by the sulforhodamine-B (SRB) assay. Different concentrations of cisplatin at 4, 40, 400 μg/mL, and 5-FU at 1-1000 μg/mL for KKU-100 and 0.3–30 μg/mL for KKU-M214, were tested.

The chemotherapeutic drugs cisplatin and 5-FU induced apoptosis of CCA cells in a dose-dependent manner (Fig. 5A–D). Suppression of Gal-3 expression significantly enhanced drug-induced apoptosis in comparison with that of the control. Knockdown of Gal-3 expression in CCA cells significantly enhanced apoptosis induced by cisplatin at all concentrations tested ($P < 0.05$). Suppression of Gal-3 improved the action of cisplatin by approximately 10 times. Cells treated with siGal-3 or with a combination of 4 μM or 40 μM cisplatin reduced cell numbers to the same levels as cells treated with 40 μM or 400 μM cisplatin (Fig. 5A,C). Similar observations were obtained for cells treated with 5-FU (Fig. 5B,D). These results indicated that the RNAi-mediated knockdown of Gal-3 increased cell sensitivity to cisplatin- and 5-FU-induced apoptosis.

To examine whether or not the enhancement of apoptosis shown in anticancer-drug-treated Gal-3 knockdown cells was associated with Gal-3, Gal-3 overexpressing cells (pEGFP-C1-hGal3-transfected KKU-M055 cells) were treated with different concentrations of cisplatin (0.005, 0.05, 0.5 μg/mL) (Fig. 5E) and 5-FU (5, 50, 500 μg/mL) (Fig. 5F). Overexpression of Gal-3 significantly diminished the cisplatin- or 5-FU-induced apoptosis in KKU-M055 cells ($P < 0.05$).
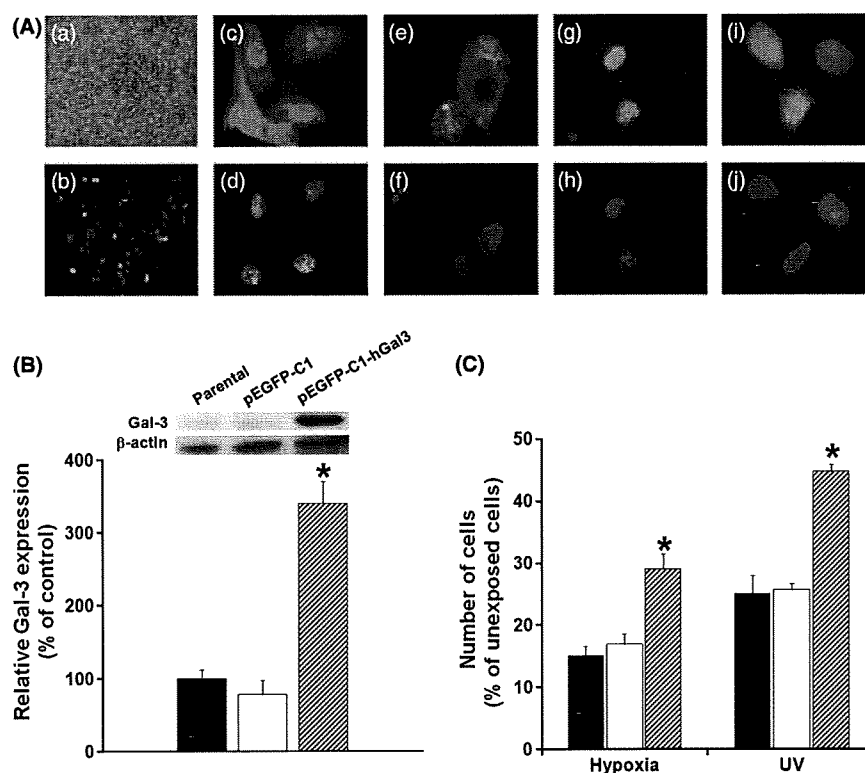
2080

Fig. 4. The anti-apoptotic activity of galectin-3 (Gal-3) was demonstrated in Gal-3 overexpressing cells. The CCA cell line, KKU-M055, was transfected with the pEGFP-C1-hGal3 vector. The efficiency of the transfection was determined by (Aa) phase contrast, (Ab) GFP-fluorescence, and (B) relative expression of Gal-3 parental and vector pEGFP-C1-transfected cells determined by Western blotting of Gal-3. The function of GFP-Gal-3 was shown to be similar to the native Gal-3 of KKU-100; (Ac,e) immunofluorescence of Gal-3 in KKU-100; (Ag,i) immunofluorescence of GFP-Gal-3 in KKU-M055 transfected with pEGFP-C1-hGal3. (Ad,f,h,j) Hoechst 33342 staining for the nucleus. Endogenous Gal-3 was prominent in the nucleus (Ac,g) and translocated to the cytoplasm under siGal-3 treatment (Ad) or short UV exposure (Ai). (C) Effects of hypoxia and UV-induced apoptosis on KKU-M055 cells, as shown by comparing Gal-3 overexpressing cells with controls. Results are the mean ± SE of three independent experiments. *P < 0.05.

Discussion

Cholangiocarcinoma (CCA) is a fatal disease with poor prognosis and high recurrence. There is no effective treatment for CCA at present, probably due to its enhanced resistance to apoptosis. Accumulated evidence indicates that Gal-3 has anti-apoptotic effects in a variety of cells.[9-13] In this study, it was demonstrated that Gal-3 played a role in anti-apoptosis; reduction of Gal-3 expression significantly induced apoptosis in CCA cells and enhanced the responsiveness of CCA cells to chemotherapeutic agents.

The present study successfully established the RNA interference (RNAi)–mediated knockdown of Gal-3 and an overexpression system for Gal-3 in CCA cell lines. The anti-apoptotic activity of Gal-3 is dependent on the expression level of endogenous Gal-3. Apoptosis was dramatically induced in CCA cells in which Gal-3 expression was diminished to baseline levels with siGal-3-K626, whereas cells treated with siGal-3-K402 which suppressed Gal-3 expression to 50%, did not induce apoptosis. Further experiment is needed to explore the mechanism that induces apoptosis in our model. However, there are a few reports related to the apoptotic pathway induced by Gal-3 depletion. Inhibition of the phosphatidylinositol-3-kinase (PI3K)/Akt signaling pathway was shown to be involved in siGal-3-treated human papillary thyroid cancer cells.[20] Gal-3 also plays role in the Wnt/β-catenin pathway. siRNA silencing of Gal-3 expression inhibited T-cell factor (TCF)-receptor activity, decreased cytosolic β-catenin level, and induced apoptosis in human colorectal cancer cells.[21]

A reduction in the anti-apoptotic activity of Gal-3 in siGal-3-K402-treated cells, however, was readily observable when the cells were exposed to hypoxia or UV-induced apoptotic conditions. Conversely, cells with overexpression of endogenous Gal-3 resisted the above two apoptotic insults. This observation indicated that the GFP-Gal-3 protein produced in Gal-3-overexpressing cells was effectively active.

The correlation of anti-apoptotic activity to the level of Gal-3 expression was also demonstrated in this study. CCA cell line KKU-100, with high endogenous Gal-3, showed higher resistance to apoptotic inductions than did KKU-OCA17 and KKU-M055, which both had lower endogenous Gal-3. These findings suggest the possibility of using expression level of Gal-3 to predict the anti-apoptotic potential of cancer cells or tissues toward chemotherapeutic drugs. This suggestion is supported by the evidence that CCA with high expression of Gal-3 exhibited high chemoresistance whereas those with low expression of Gal-3 were chemosensitive. Among the five human intrahepatic CCA cell lines (KKU-100, KKU-M055, KKU-M156, KKU-M214, and KKU-OCA17), CCA cell line KKU-100, with the highest Gal-3 expression, was highly resistant to all the chemotherapeutic drugs tested, whereas KKU-M055, which does not express Gal-3 constitutively, was the most sensitive.[22] However, this suggestion is a correlative observation and further experimental studies would be needed for a definitive conclusion.

Galectin-3 (Gal-3) seems to be a common key for the anti-apoptotic phenomenon in biological systems. As shown in this study, despite the apoptotic inducers, for example hypoxia and UV irradiation, reduction of Gal-3 expression significantly
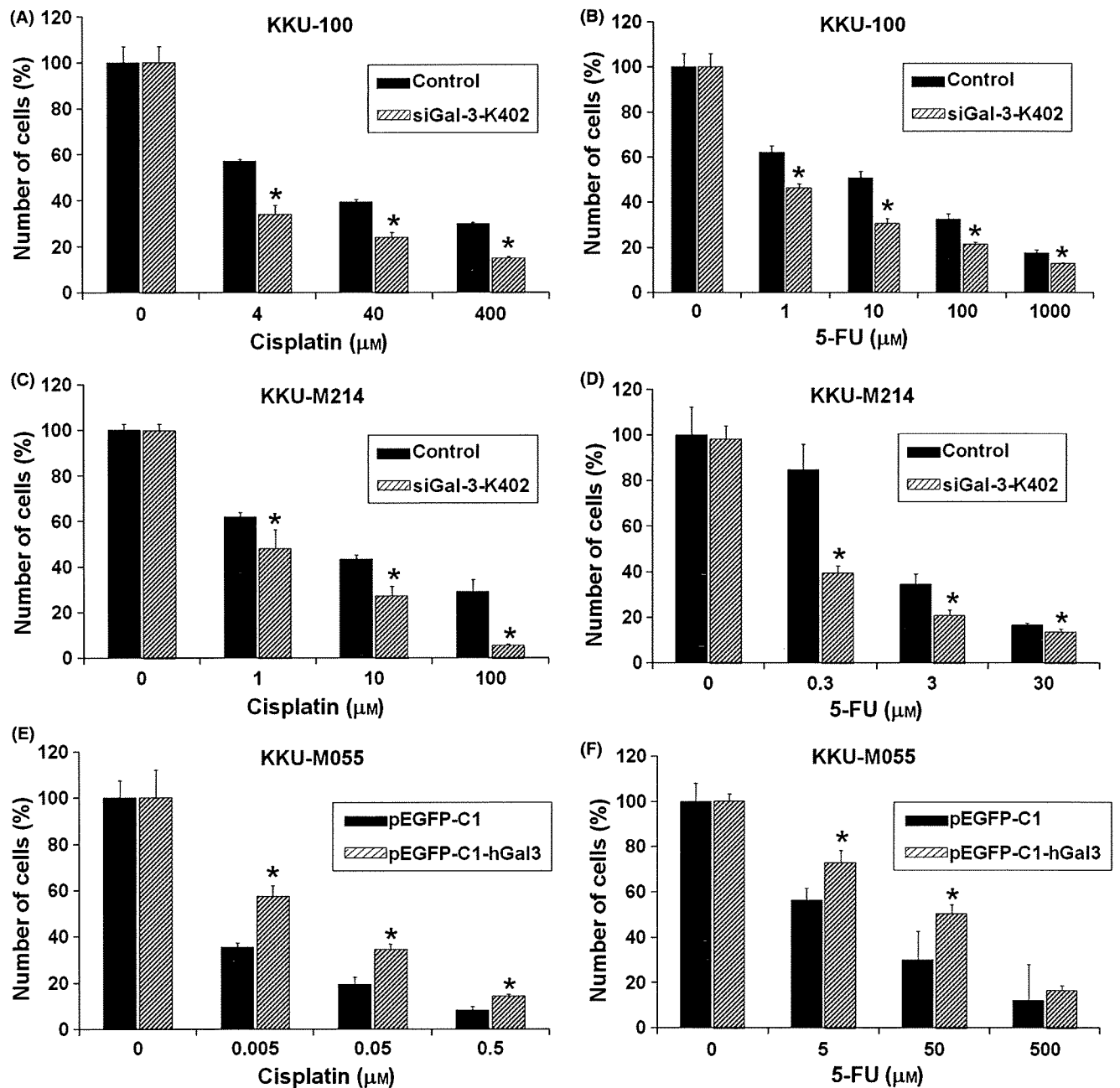
Fig. 5. Galectin-3 (Gal-3) depletion enhances anticancer drug sensitivity whereas overexpressing Gal-3 increases drug resistance. Cholangiocarcinoma (CCA) cell lines KKU-100 or KKU-M214 were treated with either Lipofectamine (black bar) or siGal-3-K402 (slash bar) for 24 h, followed by treatments with various concentrations of cisplatin (A,C) or 5-fluorouracil (5-FU) (B,D) for a further 48 h. KKU-M055 cells were treated with pEGFP-C1 (control, black bar) or pEGFP-C1-hGal3 (Gal-3 overexpressing cells, slash bar) for 24 h, followed by treatments with various concentrations of cisplatin (E) or 5-FU (F) for a further 48 h as above. The number of cells was determined by sulforhodamine-B (SRB) assay. Results are the mean ± SE (bars) of three independent experiments. *P < 0.05.

enhances apoptosis cell death of CCA cells in both conditions. In addition to our study, the anti-apoptotic action of Gal-3 in response to different apoptotic stimulations, anti-Fas-induced cell death and anoikis induced apoptosis, have been reported in B-cell lymphocytes[23] and human breast epithelial cells,[10] respectively.

The finding that Gal-3 plays a role in the anti-apoptosis of CCA cells led to further evaluation as to whether reduction of Gal-3 expression in CCA cells affected their response to the pro-apoptotic action of chemotherapeutic agents. The combined effects of siGal-3 and two chemotherapeutic agents, cisplatin and 5-FU, widely used anticancer agents frequently provided to

CCA patients, were evaluated in two CCA cell lines. As expected, the RNAi-mediated knockdown of Gal-3 synergistically enhanced the cytotoxicity of cisplatin and 5-FU in both CCA cell lines. Gal-3 knockdown by RNAi might reduce the anti-apoptotic activity and hence enhance the cytotoxicity of these anticancer drugs. The direct association of Gal-3 suppression with the enhancement of antitumor efficacy was shown in cells overexpressing Gal-3. Increasing Gal-3 expression in KKU-M055 reduced the apoptotic response to anticancer drugs. The nuclear export of phosphorylated galectin-3,[24] translocation of Gal-3 to the perinuclear membrane, and enrichment of Gal-3 in mitochondria[25] have been shown to be the mechanism

by which galectin-3 regulates its anti-apoptotic activity in response to cisplatin in the BT-549 human breast carcinoma cell line. In the present study, the translocation of Gal-3 from the nucleus to cytoplasm was also observed under apoptotic insult. More experimental data are needed to indicate the definite mechanism by which Gal-3 exerted its anti-apoptotic activity in our study.

Galectin-3 (Gal-3) contains the NWGR (N, asparagine; W, tryptophan; G, glycine; R, arginine) anti-death motif of the Bcl-2 family. One of the mechanisms by which Gal-3 acts on anti-apoptosis in response to anticancer drugs has been shown to be the stimulation of Bcl-2 associated death (Bad) protein phosphorylation and decreasing Bad expression, which resulted in the stabilization of mitochondrial membrane integrity, and subsequently the inhibition of cytochrome c release and caspase-3 activation, which finally suppressed apoptosis.[26] Additionally, an anti-apoptotic effect of Gal-3, which is meditated by the activation of the extracellular signal-regulated kinases (ERK) and c-Jun NH_2-terminal kinase (JNK) pathways, is also suggested.[27] The overexpression of Gal-3 probably protects cells from apoptotic death by inhibiting the caspase pathway,[9] or by maintaining mitochondrial homeostasis.[28]

Resistance to chemotherapeutic agents is the major cause of failure for anticancer drug treatment in many cancers, including CCA. Thymidilate synthase, multidrug resistant protein (MRP1), multidrug resistant-associated proteins (MDR3), and glutathione-S-transferase 1 (GSTP1) are highly expressed in several CCA cell lines, including KKU-100 and KKU-M214.[22] The actions of these genes may underline the chemo-resistant properties of CCA cells. The finding that the suppression of Gal-3 expression enhances the sensitivity of antitumor drugs suggests the possibility that Gal-3 could be a new target molecule for improving the response of CCA cells to chemotherapeutic drugs.

In conclusion, these results suggest that the expression of Gal-3 provides tumor cells with an anti-apoptotic advantage. Cells with high expression of Gal-3 tend to resist chemotherapeutic treatment, whereas cells with low Gal-3 expression are prone to apoptosis, and hence are sensitive to drug treatment. Based on this observation, Gal-3 expression levels in cancer tissue may be a predictor of chemotherapeutic response, which could help clinicians select an appropriate treatment for CCA patients. Several approaches have been developed to reduce cellular Gal-3 expression. For instance, siGal-3 may be delivered into solid tumors by an efficient delivery system of siRNA[29] that is becoming a conventional application for *in vivo* cancer therapy.[30,31] Synthetic lactulose amines, for example lactulosyl-L-leucine and modified citrus pectin, have been designed and shown to be specific Gal-3 inhibitors for therapeutic purposes.[32] The treatment of cells with modified citrus pectin and lactulosyl-L-leucine was able to abrogate resistance to doxorubicin in angiosarcoma cells.[33] Moreover, the inhibition of Gal-3 anti-apoptotic function by modified citrus pectin was sufficient to reverse multiple myeloma cells' resistance to bortezomib, and enhance their response to apoptosis induced by dexamethasone.[34] Since Gal-3 is frequently expressed in CCA tissues, it is therefore proposed that interfering with Gal-3 action, either by using RNAi-mediated knockdown of Gal-3, or specific Gal-3 inhibitors, can either be developed as a specific gene-targeting therapy to treat CCA, or used in combination with a chemotherapeutic agent to enhance apoptosis and chemosensitivity in CCA.

Acknowledgments

References

1 Vatanasapt V, Tangvoraphonkchai V, Titapant V, Pipitgool V, Viriyapap D, Sriamporn S. A high incidence of liver cancer in Khon Kaen Province, Thailand. *Southeast Asian J Trop Med Public Health* 1990; **21**: 489–94.

2 Haswell-Elkins MR, Mairiang E, Mairiang P *et al.* Cross-sectional study of *Opisthorchis viverrini* infection and cholangiocarcinoma in communities within a high-risk area in northeast Thailand. *Int J Cancer* 1994; **59**: 505–9.

3 Thongprasert S. The role of chemotherapy in cholangiocarcinoma. *Ann Oncol* 2005; **16** (Suppl 2): ii, 93–6.

4 Junking M, Wongkham C, Sripa B, Sawanyawisuth K, Araki N, Wongkham S. Decreased expression of galectin-3 is associated with metastatic potential of liver fluke-associated cholangiocarcinoma. *Eur J Cancer* 2008; **44**: 619–26.

5 Barondes SH, Cooper DN, Gitt MA, Leffler H. Galectins. Structure and function of a large family of animal lectins. *J Biol Chem* 1994; **269**: 20807–10.

6 Hirabayashi J, Kasai K. The family of metazoan metal-independent beta-galactoside-binding lectins: structure, function and molecular evolution. *Glycobiology* 1993; **3** (4): 297–304.

7 Hughes RC. Galectins as modulators of cell adhesion. *Biochimie* 2001; **83**: 667–76.

8 Yang RY, Liu FT. Galectins in cell growth and apoptosis. *Cell Mol Life Sci* 2003; **60**: 267–76.

9 Akahani S, Nangia-Makker P, Inohara H, Kim HR, Raz A. Galectin-3: a novel antiapoptotic molecule with a functional BH1 (NWGR) domain of Bcl-2 family. *Cancer Res* 1997; **57** (23): 5272–6.

10 Kim HR, Lin HM, Biliran H, Raz A. Cell cycle arrest and inhibition of anoikis by galectin-3 in human breast epithelial cells. *Cancer Res* 1999; **59** (16): 4148–54.

11 Lin HM, Moon BK, Yu F, Kim HR. Galectin-3 mediates genistein-induced G(2)/M arrest and inhibits apoptosis. *Carcinogenesis* 2000; **21**: 1941–5.

12 Yang RY, Hsu DK, Liu FT. Expression of galectin-3 modulates T-cell growth and apoptosis. *Proc Natl Acad Sci U S A* 1996; **93** (13): 6737–42.

13 Yoshii T, Fukumori T, Honjo Y, Inohara H, Kim HR, Raz A. Galectin-3 phosphorylation is required for its anti-apoptotic function and cell cycle arrest. *J Biol Chem* 2002; **277** (9): 6852–7.

14 Hsu DK, Yang RY, Pan Z *et al.* Targeted disruption of the galectin-3 gene results in attenuated peritoneal inflammatory responses. *Am J Pathol* 2000; **156** (3): 1073–83.

15 Sripa B, Leungwattanawanit S, Nitta T *et al.* Establishment and characterization of an opisthorchiasis-associated cholangiocarcinoma cell line (KKU-100). *World J Gastroenterol* 2005; **11** (22): 3392–7.

16 Elbashir SM, Harborth J, Weber K, Tuschl T. Analysis of gene function in somatic mammalian cells using small interfering RNAs. *Methods* 2002; **26**: 199–213.

17 Laemmli UK. Cleavage of structural proteins during the assembly of the head of bacteriophage T4. *Nature* 1970; **227** (5259): 680–5.

18 Towbin H, Staehelin T, Gordon J. Electrophoretic transfer of proteins from polyacrylamide gels to nitrocellulose sheets: procedure and some applications. *Proc Natl Acad Sci U S A* 1979; **76** (9): 4350–4.

19 Skehan P, Storeng R, Scudiero D *et al.* New colorimetric cytotoxicity assay for anticancer-drug screening. *J Natl Cancer Inst* 1990; **82** (13): 1107–12.

20 Lin CI, Whang EE, Abramson MA *et al.* Galectin-3 regulates apoptosis and doxorubicin chemoresistance in papillary thyroid cancer cells. *Biochem Biophys Res Commun* 2009; **379**: 626–31.

21 Shi Y, He B, Kuchenbecker KM *et al.* Inhibition of Wnt-2 and galectin-3 synergistically destabilizes beta-catenin and induces apoptosis in human colorectal cancer cells. *Int J Cancer* 2007; **121**: 1175–81.

22 Tepsiri N, Chaturat L, Sripa B *et al.* Drug sensitivity and drug resistance profiles of human intrahepatic cholangiocarcinoma cell lines. *World J Gastroenterol* 2005; **11** (18): 2748–53.

23 Hoyer KK, Pang M, Gui D *et al.* An anti-apoptotic role for galectin-3 in diffuse large B-cell lymphomas. *Am J Pathol* 2004; **164** (3): 893–902.

24 Takenaka Y, Fukumori T, Yoshii T *et al.* Nuclear export of phosphorylated galectin-3 regulates its antiapoptotic activity in response to chemotherapeutic drugs. *Mol Cell Biol* 2004; **24**: 4395–406.

25 Yu F, Finley RL Jr, Raz A, Kim HR. Galectin-3 translocates to the perinuclear membranes and inhibits cytochrome c release from the mitochondria. A role for synexin in galectin-3 translocation. *J Biol Chem* 2002; **277**: 15819–27.

26 Fukumori T, Oka N, Takenaka Y *et al.* Galectin-3 regulates mitochondrial stability and antiapoptotic function in response to anticancer drug in prostate cancer. *Cancer Res* 2006; **66** (6): 3114–9.

27 Fukumori T, Takenaka Y, Yoshii T *et al.* CD29 and CD7 mediate galectin-3-induced type II T-cell apoptosis. *Cancer Res* 2003; **63** (23): 8302–11.

28 Matarrese P, Tinari N, Semeraro ML, Natoli C, Iacobelli S, Malorni W. Galectin-3 overexpression protects from cell damage and death by influencing mitochondrial homeostasis. *FEBS Lett* 2000; **473**: 311–5.

29 Takei Y, Kadomatsu K, Yuzawa Y, Matsuo S, Muramatsu T. A small interfering RNA targeting vascular endothelial growth factor as cancer therapeutics. *Cancer Res* 2004; **64** (10): 3365–70.

30 Hingorani SR, Jacobetz MA, Robertson GP, Herlyn M, Tuveson DA Suppression of BRAF(V599E) in human melanoma abrogates transformation *Cancer Res* 2003; **63** (17): 5198–202.

31 Brummelkamp TR, Bernards R, Agami R. Stable suppression o tumorigenicity by virus-mediated RNA interference. *Cancer Cell* 2002; **2** 243–7.

32 Rabinovich GA, Cumashi A, Bianco GA *et al.* Synthetic lactulose amines novel class of anticancer agents that induce tumor-cell apoptosis and inhibi galectin-mediated homotypic cell aggregation and endothelial cel morphogenesis. *Glycobiology* 2006; **16** (3): 210–20.

33 Johnson KD, Glinskii OV, Mossine VV *et al.* Galectin-3 as a potentia therapeutic target in tumors arising from malignant endothelia. *Neoplasia (New York, NY)* 2007; **9** (8): 662–70.

34 Chauhan D, Li G, Podar K *et al.* A novel carbohydrate-based therapeutic GCS-100 overcomes bortezomib resistance and enhances dexamethasone induced apoptosis in multiple myeloma cells. *Cancer Res* 2005; **65** (18) 8350–8.

Supporting Information

Additional Supporting Information may be found in the online version of this article:

Fig. S1. Cholangiocarcinoma (CCA) cell line KKU-100 cells were transfected with siGal-3-K626 and the endogenous galectin-3 (Gal-3) was determined by immunoblotting after siRNA transfection for 6, 24, 48, and 72 h. Expression of Gal-3 was gradually suppressed and the effect of siRNA was observed at 6 h before apoptotic induction.

Please note: Wiley-Blackwell are not responsible for the content or functionality of any supporting materials supplied by the authors. Any queries (other than missing material) should be directed to the corresponding author for the article.

Silver Ion Unusually Stabilizes the Structure of a Parallel-Motif DNA Triplex

Toshihiro Ihara,*,†,§ Tatsuaki Ishii,† Norie Araki,‡ Anthony W. Wilson,‡ and Akinori Jyo†

Graduate School of Science and Technology, Kumamoto University, 2-39-1 Kurokami, Kumamoto 860-8555, Japan, Graduate School of Medical Sciences, Kumamoto University, 1-1-1 Honjo, Kumamoto 860-8556, Japan, and PRESTO, Japan Science and Technology Agency, San-bancho Building, 3-5 Sanbancho, Chiyodaku, Tokyo 332-0012, Japan

Received December 12, 2008; E-mail: toshi@chem.kumamoto-u.ac.jp

The DNA triple helix is one of the most useful recognition motifs in the design of systems for sequence-specific labeling, regulation of gene expression, and construction of DNA-based nanostructures.[1] It can form in two main ways: an oligopyrimidine strand can bind to the major groove of the duplex parallel to the strand carrying the purine tract using Hoogsteen base-pairing, or alternatively, an oligopurine can bind to the purine strand in an antiparallel orientation using reversed Hoogsteen base-pairing. In the parallel motif, cytosines in the third strand need to be protonated at their N3 positions ($pK_a = 4.5$) to form CG.C$^+$ base triplets, which stabilize the triplex by favorable electrostatic effects. Therefore, the stability of triplexes containing CG.C$^+$ largely depends on the pH of the solution. While it is more stable than those consisting entirely of TA.T triplets in weakly acidic solution, its stability is very low under physiological conditions.

Several research groups have devoted their efforts to improving the stability of the triplex at neutral pH.[2] These efforts fall into two categories: (1) addition or covalent attachment of auxiliary molecules that alleviate the electrostatic repulsion between the strands or act as a nonspecific anchor[3] and (2) redesign of the DNA backbone and bases.[4] Here we report an effective alternative method for stabilization of the parallel-motif triple helix of DNA using Ag$^+$ ions. To date, several oligodeoxyribonucleotide (ODN) conjugates carrying metal-chelating moieties have been synthesized.[5] Their binding with the targets was regulated by appropriate metal ions through the specific coordination of the appended chelators. Recently, Ono and co-workers[6] reported that the formation of C−C and T−T mispairings in the duplex are promoted by Ag$^+$ and Hg^{2+}, respectively. In the duplexes, the ions were placed between the bases to form specific bridges (C−Ag$^+$−C, T−Hg^{2+}−T). We report the effect of Ag$^+$ on the stability of triplexes containing CG.C$^+$ base triplets. The silver ion is expected to displace an N3 proton of a cytosine in the CG.C$^+$ base triplet to form a CG.CAg$^+$, as shown in Figure 1A. This would stabilize parallel-motif triplexes even at neutral pH.

The sequences of ODNs used in this study are shown in Figure 1B. First, UV melting experiments were carried out for the triplexes T11/A11/T11 and TC11/AG11/TC11 at pH 8.5 in the absence and the presence of Ag$^+$.[7] T11/A11/T11 consists of 11 TA.T triplets. Only the central TA.T triplet was displaced by a CG.C$^+$ in TC11/AG11/TC11. The melting curves are shown in Figure 2A. The meltings of the triplexes could be resolved in two steps in the absence of Ag$^+$. The transitions at lower and higher temperatures are attributed to triplex−duplex (t−d) and duplex−coil (d−c) transitions, respectively. Upon addition of Ag$^+$ to TC11/AG11/TC11, the t−d transition almost disappeared and merged with the d−c transition. Although this effect was already significant when an equimolar amount of Ag$^+$ for the
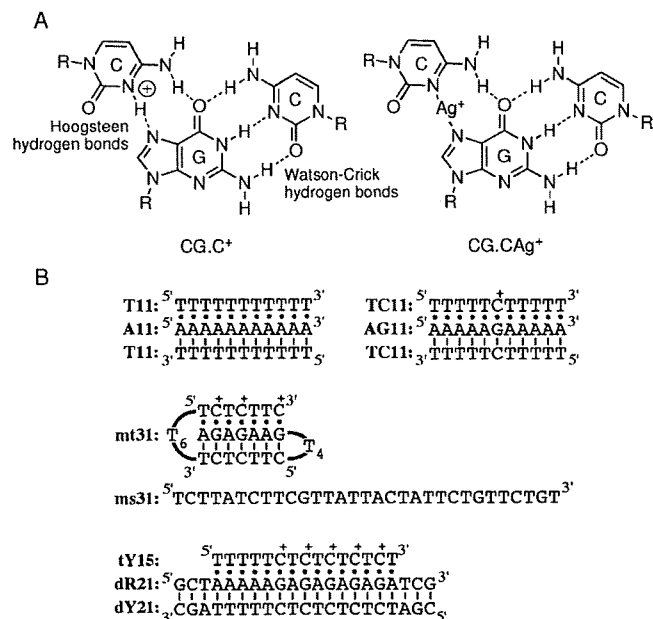
† Graduate School of Science and Technology, Kumamoto University.
‡ Graduate School of Medical Sciences, Kumamoto University.
§ PRESTO.

Figure 1. (A) CG.C$^+$ base triplet and the Ag$^+$-mediated base triplet CG.CAg$^+$. (B) Sequences of ODNs used in this study. Bars and dots show Watson−Crick and Hoogsteen base pairings, respectively.
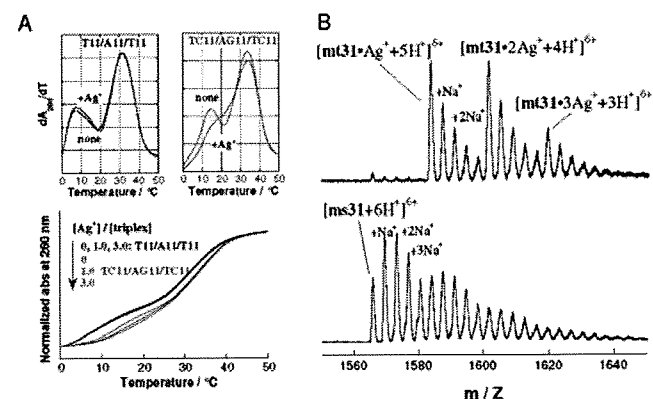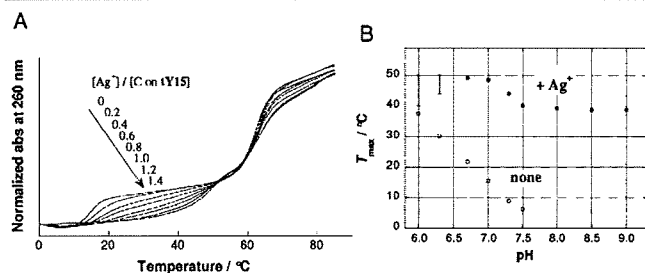

Figure 2. (A) UV melting curves of the triple helixes T11/A11/T11 (black) and TC11/AG11/TC11 (red). Each strand (2.5 μM) was dissolved in phosphate buffer (10 mM, pH 8.5) containing 200 mM NaNO$_3$ and 0, 2.5, or 7.5 μM AgNO$_3$. (top) First derivatives of the melting curves obtained in the absence and presence of 7.5 μM Ag$^+$; (bottom) the melting curves. (B) ESI-TOF mass spectra of (top) mt31 and (bottom) ms31 in the presence of 1.5 times the amount of Ag$^+$ for possible CG.C$^+$ triplets.

CG.C$^+$ triplet was added, the shape of the curve around the t−d transition showed a further slight change with additional Ag$^+$. On the other hand, the melting curve of T11/A11/T11 was scarcely changed by Ag$^+$ titration. Silver ions did not affect the d−c transitions for either

Figure 3. (A) UV melting curves of **dY21/dR21/tY15** obtained in the presence of various amounts of Ag$^+$. Each strand (2.5 μM) was dissolved in phosphate buffer (10 mM, pH 7.0) containing 200 mM NaNO$_3$ and 0−17.5 μM AgNO$_3$. (B) pH dependence of T_{max} of the t−d transition of **dY21/dR21/tY15** melting in the absence (O) and presence (●) of an equimolar amount of Ag$^+$ for cytosines in **tY15**.

triplex. Therefore, Ag$^+$ seems to work only on Hoogsteen hydrogen bonding in the CG.C$^+$ triplet.

To confirm the specific interaction between CG.C$^+$ and Ag$^+$, **mt31**, which forms an intramolecular triplex structure containing three CG.C$^+$ structures, was subjected to mass spectrometry [(nano)ESI-QqTOF] in the presence of 1.5 times the amount of Ag$^+$ for the CG.C$^+$ triplet. The spectra are shown in Figure 2B. Almost all of the **mt31** was detected as Ag adducts with a discrete number of Ag$^+$ (**mt31·Ag$^+$**, **mt31·2Ag$^+$**, and **mt31·3Ag$^+$**). On the other hand, the control 31-mer ODN **ms31** with a scrambled sequence was mainly detected as several Na adducts of Ag$^+$-free forms under exactly the same conditions as for **mt31**. The sequence of **ms31** was designed to not form the intramolecular triplex with CG.C$^+$ triplets. These results suggest the specific (but probably not very strong) interaction of Ag$^+$ with CG.C$^+$ triplets.

The effect of Ag$^+$ on the stability of the triplex was investigated using the triplex **dY21/dR21/tY15** having multiple CG.C$^+$ triplets in the sequence. UV melting experiments were performed at pH 7.0 in the presence of various amounts of Ag$^+$ (Figure 3A). Silver ions raised the temperature of the t−d transition, T_{max}, with significant broadening, and eventually, at the equimolar point with cytosine, a new inflection point appeared at 48.7 °C.[8] The stabilization effect of Ag$^+$ on the binding of the third strand (**tY15**), ΔT_{max}, was more than 30 °C (48.7−16.8 °C). Meanwhile the d−c transition was scarcely affected by Ag$^+$ addition in this concentration range. This implies that an Ag$^+$−triplex complex with a certain structure that has its own quite high thermal stability forms at the equimolar point and that in the complex, Ag$^+$ only affects Hoogsteen base-pairing of CG.C$^+$ triplets. The pH effect on T_{max} was monitored in the absence and the presence of Ag$^+$. Although T_{max} steadily decreased with rising pH in the absence of Ag$^+$, the T_{max} values observed in the presence of Ag$^+$ showed a unique biphasic behavior consisting of two pH-independent regions.[9] The slope of the T_{max}-versus-pH plot is related to the number of protons released when the structures melt to give other forms in equilibrium. As we expected, Ag$^+$ would displace the N3 proton of cytosine in CG.C$^+$ to form a new triplet, CG.CAg$^+$, below pH 7. Meanwhile, the proton of the exocyclic amino group of cytosine is considered to be dissociated at pH > 7.0 in the presence of Ag$^+$.[10] Therefore, another pH-independent equilibrium between CG.C$^-$Ag$^+$ and CG + C$^-$Ag$^+$ would work in the t−d transition at pH > 8.0. The broadening observed in the transitions before Ag$^+$ saturation would be derived from the mixture of the triplexes that contain various numbers of Ag$^+$ on cytosines at different positions, because each of the triplexes should have its own intrinsic thermal stability. Therefore, silver ions are probably incorporated fairly independently into the five binding pockets in **dY21/dR21/tY15** in a saturation process.

To obtain information about the triplex structures, **dY21/dR21/ tY15** was subjected to CD measurements [see the Supporting Information (SI)]. While the spectra measured at 7 and 27 °C in the absence of Ag$^+$ were different, especially in the region of short wavelengths, the corresponding spectra were essentially the same in the presence of Ag$^+$. This is consistent with the results of the melting experiments shown in Figure 3A. However, the shapes of the CD spectra in the presence of Ag$^+$ were quite different from the typical spectra of DNA triplexes. The coordination distance in N−Ag$^+$−N would be longer than that of the Hoogsteen hydrogen bonds in CG.C$^+$. Model studies show that the cytosines on the third strand are forced to be twisted from the plane of Watson−Crick GC pairs in CG.CAg$^+$ triplets (see the SI). This nonplanarity of five CG.CAg$^+$ triplets in **dY21/dR21/tY15** seems to unusually alter the whole structure of the triple helix.

We have shown that Ag$^+$ remarkably stabilizes the structure of a parallel-motif DNA triplex. Several ligands that specifically bind with DNA triplexes have been developed.[3a,b] The stabilization effect of Ag$^+$ favorably compares with those for these ligands. This very simple method would be a good choice for the stabilization of DNA triplexes, especially in vitro.
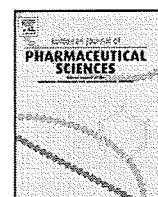
Supporting Information Available: Additional melting curves and CD spectra of **dY21/dR21/tY15** and the results of DFT calculations for the Ag$^+$-mediated base triplets. This material is available free of charge via the Internet at http://pubs.acs.org

References

(1) Soyfer, V. N.; Potaman, V. N. *Triple-Helical Nucleic Acids*; Springer: New York, 1995.

(2) Rusling, D. A.; Brown, T.; Fox, K. R. In *Sequence-Specific DNA Binding Agents*; Waring, M., Ed.; RSC Publishing: Cambridge, U.K., 2006; pp 1−22.

(3) (a) Pilch, D. S.; Breslauer, K. J. *Proc. Natl. Acad. Sci. U.S.A.* **1994**, *91*, 9332−9336. (b) Silver, G. C.; Sun, J.-S.; Nguyen, C. H.; Boutorine, A. S.; Bisagni, E.; Hélène, C. *J. Am. Chem. Soc.* **1997**, *119*, 263−268. (c) Li, H.; Broughton-Head, V. J.; Peng, G.; Power, V. E. C.; Ovens, M. J.; Fox, K. R.; Brown, T. *Bioconjugate Chem.* **2006**, *17*, 1561−1567.

(4) (a) Kumar, N.; Nielsen, K. E.; Maiti, S.; Petersen, M. *J. Am. Chem. Soc.* **2006**, *128*, 14−15. (b) Alam, M. R.; Majumdar, A.; Thazhathveetil, A. K.; Liu, J.-L.; Puri, N.; Cuenoud, B.; Sasaki, S.; Miller, P. S.; Seidman, M. M. *Biochemistry* **2007**, *46*, 10222−10233. (c) Rahman, S. M. A.; Seki, S.; Obika, S.; Haitani, S.; Miyashita, K.; Imanishi, T. *Angew. Chem., Int. Ed.* **2007**, *46*, 4306−4309. (d) Shinozuka, K.; Matsumoto, N.; Suzuki, H.; Moriguchi, T.; Sawai, H. *Chem. Commun.* **2002**, 2712−2713.

(5) (a) Tanaka, K.; Tengeiji, A.; Kato, T.; Toyama, N.; Shionoya, M. *Science* **2003**, *299*, 1212−1213. (b) Clever, G. H.; Carell, T. *Angew. Chem., Int. Ed.* **2007**, *46*, 250−253. (c) Kitamura, Y.; Ihara, T.; Tsujimura, Y.; Osawa, Y.; Sasahara, D.; Yamamoto, Y.; Okada, K.; Tazaki, M.; Jyo, A. *J. Inorg. Biochem.* **2008**, *102*, 1921−1931. (d) Ihara, T.; Takeda, Y.; Jyo, A. *J. Am. Chem. Soc.* **2001**, *123*, 1772−1773. (e) Ihara, T.; Sato, Y.; Shimada, H.; Jyo, A. *Nucleosides, Nucleotides Nucleic Acids* **2008**, *27*, 1084−1096.

(6) (a) Miyake, Y.; Togashi, H.; Tashiro, M.; Yamaguchi, H.; Oda, S.; Kudo, M.; Tanaka, Y.; Kondo, Y.; Sawa, R.; Fujimoto, T.; Machinami, T.; Ono, A. *J. Am. Chem. Soc.* **2006**, *128*, 2172−2173. (b) Ono, A.; Cao, S.; Togashi, H.; Tashiro, M.; Fujimoto, T.; Machinami, T.; Oda, S.; Miyake, Y.; Okamoto, I.; Tanaka, Y. *Chem. Commun.* **2008**, 4825−4827.

(7) We first attempted the melting experiments at pH 7. However, the triplex TC11/AG11/TC11 melted almost cooperatively. To evaluate both transitions (t−d and d−c) separately, the pH was raised to 8.5.

(8) The maximum temperatures of the first derivative of the melting curves, T_{max}, were used as the indicators of triplex stabilities.

(9) T_{max} values around pH 6 were not precisely determined because the t−d transitions became broad, as in the melting curves before Ag$^+$ saturation measured at pH 7 (Figure 3A). However, the curves became sharper upon further addition of Ag$^+$ (2 times for C). This supports the idea of proton displacement by Ag$^+$ in the CG.C$^+$ base triplet.

(10) (a) Daune, M.; Dekker, C. A.; Schachman, H. K. *Biopolymers* **1966**, *4*, 51−76. (b) Eichhorn, G. L.; Butzow, J. J.; Clark, P. *Biopolymers* **1966**, *5*, 283−296.

JA809702N

Contents lists available at ScienceDirect

European Journal of Pharmaceutical Sciences

Involvement of PI3K-Akt-Bad pathway in apoptosis induced by 2,6-di-O-methyl-β-cyclodextrin, not 2,6-di-O-methyl-α-cyclodextrin, through cholesterol depletion from lipid rafts on plasma membranes in cells

Keiichi Motoyama[a], Kazuhisa Kameyama[a], Risako Onodera[a], Norie Araki[b], Fumitoshi Hirayama[c], Kaneto Uekama[c], Hidetoshi Arima[a,*]

[a] Graduate School of Pharmaceutical Sciences, Kumamoto University, 5-1 Oe-honmachi, Kumamoto 862-0973, Japan
[b] Graduate School of Medical Sciences, Kumamoto University, Kumamoto 860-8556, Japan
[c] Faculty of Pharmaceutical Sciences, Sojo University, Kumamoto 860-0082, Japan

ABSTRACT

Cyclodextrins (CyDs), which are widely used to increase the solubility of drug in pharmaceutical fields, are known to induce hemolysis and cytotoxicity at high concentrations. However, it is still not unclear whether cell death induced by CyDs is apoptosis or not. Therefore, in the present study, we investigated the effects of various kinds of CyDs on apoptosis in the cells such as NR8383 cells, A549 cells and Jurkat cells. Of various CyDs, methylated CyDs inducted cell death under the present experimental conditions, but hydroxypropylated CyDs or sulfobutyl ether-β-CyD (SBE7-β-CyD) did not. Of methylated CyDs, 2,6-di-O-methyl-β-cyclodextrin (DM-β-CyD) and 2,3,6-tri-O-methyl-β-cyclodextrin (TM-β-CyD) markedly caused apoptosis in NR8383 cells, A549 cells and Jurkat cells, through cholesterol depletion in cell membranes. In sharp contrast, 2,6-di-O-methyl-α-cyclodextrin (DM-α-CyD) and methyl-β-cyclodextrin (M-β-CyD) induced cell death in an anti-apoptotic mechanism. DM-β-CyD induced apoptosis through the inhibition of the activation of PI3K-Akt-Bad pathway. Neither p38 MAP kinase nor p53 was contributed to the induction of apoptosis by DM-β-CyD. Additionally, DM-β-CyD significantly decreased mitochondrial transmembrane potential, and then caused the release of cytochrome c from mitochondria to cytosol in NR8383 cells. Furthermore, we confirmed that down-regulation of pro-caspase-3 and activation of caspase-3 after incubation with DM-β-CyD. These results suggest that of methylated CyDs, DM-β-CyD, not DM-α-CyD, induces apoptosis through the PI3K-Akt-Bad pathway, resulting from cholesterol depletion in lipid rafts of cell membranes.

© 2009 Elsevier B.V. All rights reserved.

1. Introduction

There are three forms of cell death: apoptosis, autophagic cell death, and necrosis (Edinger and Thompson, 2004). Recently, the additional form of cell death, a programmed necrosis, has been reported (Zong et al., 2004; Tu et al., 2009). Among the four distinct forms of cell death, apoptosis is best studied. Apoptosis is roughly defined by morphological and biochemical changes of the cells (Allen et al., 1997; Taatjes et al., 2008; Loos and Engelbrecht, 2009). Two distinct apoptotic signaling pathways, i.e. mitochondrial-dependent and -independent pathways control apoptosis activation. Intracellular cues, such as damage to the cell's DNA, drive apoptosis primarily through the

mitochondrial-dependent pathway, while extracellular signals, usually generated by cytotoxic cells of immune system, trigger apoptosis mainly through the mitochondrial-independent pathway (Ashkenazi, 2008). Both pathways stimulate pro-apoptotic caspase, a family of cysteine proteases, as pro-caspases and are activated through a process called 'the caspase cascade' (Kim et al., 2005; Lavrik et al., 2005).

Membrane lipids are known to be associated with cell death. Cholesterol is an abundant component of the plasma membrane of eukaryotic cells, which plays a pivotal role in the regulation of membrane fluidity, permeability, receptor function and ion channel activity (Brown and London, 1998; Burger et al., 2000; Simons and Toomre, 2000; Edidin, 2003). The lateral distribution of cholesterol in the membrane is not uniform and its content is particularly high in lipid rafts (Dobrowsky, 2000). These microdomains have been reported to act as molecular platforms that spatially organize membrane receptor molecules such as epidermal growth factor
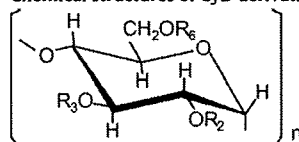

(EGF) receptor and CD95 (Fas) (Simons and Toomre, 2000; Dykstra et al., 2003; Bollinger et al., 2005). This reorganization is of crucial importance in the initiation and regulation of inflammatory processes and apoptosis. For example, redistribution of death receptors such as Fas to cholesterol-enriched lipid domains has been proposed to be an important regulatory step during the activation of the apoptotic death program (Grassme et al., 2001; Lacour et al., 2004). Meanwhile, phosphoinositides such as phosphatidylinositol 3,4,5-trisphosphate and phosphatidylinositol 3,4-bisphosphate promote cell survival and protect against apoptosis by activating Akt/PKB, which phosphorylates components of the apoptotic machinery (Mejillano et al., 2001). In addition, ceramides which serve as intermediates for sphingolipids, a major component of cell membranes have been implicated as signaling molecules, and in response to various stresses such as hypoxia and restricted blood supply (ischemia), total cellular ceramide concentration increases, which in turn can activate molecules that induce apoptosis (Crowder, 2009). Therefore, the regulation of membrane lipids levels in lipid rafts is one of the key factors of apoptotic signal in cells.

Cyclodextrins (CyDs) and their hydrophilic derivatives form inclusion complexes with hydrophobic molecules. CyDs can improve the solubility, dissolution rate and bioavailability of the drugs, and so the widespread use of CyDs is well known in the pharmaceutical field (Uekama et al., 1998; Szente and Szejtli, 1999). CyDs have been reported to interact with cell membrane constituents such as cholesterol and phospholipids, resulting in the induction of hemolysis of human and rabbit red blood cells (RRBC) (Irie et al., 1982; Ohtani et al., 1989; Fauvelle et al., 1997). Additionally, we have reported that CyDs-induced hemolysis at high concentration: the magnitude of hemolytic activity of CyDs in human erythrocytes increased in the order of γ-CyD < α-CyD < 2-hydroxypropyl-β-CyD (HP-β-CyD) < β-CyD < 2,3,6-tri-O-methyl-β-CyD (TM-β-CyD) < 2,6-di-O-methyl-β-CyD (DM-β-CyD) and there is a positive correlation between the hemolytic activity of CyDs and their capacity to solubilize cholesterol (Irie and Uekama, 1997).

Numerous studies regarding the disruption of lipid rafts by CyDs have been reported (Kabouridis et al., 2000; Parpal et al., 2001). It is well known that methyl-β-CyD (M-β-CyD) disrupts lipid rafts through extraction of cholesterol from cell membranes and alters cell signaling at the cell surface in cell biology (Gniadecki, 2004; Hueber et al., 2002). Recently, we reported that DM-β-CyD and M-β-CyD induced morphological change of RRBC from discocyte to echinocyte through the extraction of cholesterol from cholesterol-rich lipid rafts (Motoyama et al., 2009), while 2,6-di-O-methyl-α-CyD (DM-α-CyD) induced morphological changes from discocyte to stomatocyte by the extraction of sphingomyelin from sphingolipid-rich lipid rafts, but not extraction of cholesterol (Motoyama et al., 2009). These lines of evidence make it tempting to speculate that DM-β-CyD and DM-α-CyD show the differential type of cell death, because these CyDs extract membrane constituents from the different lipid microdomains on RRBC membranes. However, it is still not unclear whether these CyDs induce apoptosis or not through the interaction with membrane components in various kinds of cells. Therefore, in the present study, we examined whether cell death induced by CyDs is apoptosis or not toward various cells such as NR8383 cells; rat alveolar macrophage cell line, A549 cells; human lung adenocarcinoma epithelial cell line, and Jurkat cells; human T cell lymphoblast-like cell line. To gain insight into the mechanism for this apoptotic effect of DM-β-CyD, the involvement of apoptotic signaling pathways of PI3K-Akt, MAP kinase, p53, cytochrome *c* and caspase-3 in apoptosis induced by DM-β-CyD was studied. Finally, we discussed the effects of the type of lipid rafts on apoptosis and the potential use of DM-β-CyD as well as TM-β-CyD as novel antitumor agents.

Table 1
Chemical structures of CyD derivatives used in this study.

Compound	n	R2, R3, R6	DS[a]
α-CyD	6	H	–
β-CyD	7	H	–
γ-CyD	8	H	–
M-β-CyD[b]	7	H or CH$_3$	12.6
DM-α-CyD[c]	6	R$_2$, R$_6$=CH$_3$, R$_3$=H	12
DM-β-CyD[d]	7	R$_2$, R$_6$=CH$_3$, R$_3$=H	14
TM-β-CyD[e]	7	R$_2$, R$_3$, R$_6$=CH$_3$	21
HP-α-CyD[f]	6	H or CH$_2$ CH(OH)CH$_3$	4.1
HP-β-CyD[g]	7	H or CH$_2$CH(OH)CH$_3$	4.8
SBE7-β-CyD[h]	7	H or (CH$_2$)$_4$SO$_3$Na	6.2

[a] Average degree of substitution.
[b] Methyl-β-CyD.
[c] 2,6-Di-O-methyl-α-CyD.
[d] 2,6 -Di-O-methyl-β-CyD.
[e] 2,3,6-Tri-O-methyl-β-CyD.
[f] 2-Hydroxypropyl-α-CyD.
[g] 2-Hydroxypropyl-β-CyD.
[h] Sulfobutyl ether-β-CyD.

2. Materials and methods

2.1. Materials

CyDs used in the present study are depicted in Table 1. α-, β-, γ-CyD, 2-hydroxypropyl-α-CyD (HP-α-CyD), HP-β-CyD, 2-hydroxypropyl-γ-CyD (HP-γ-CyD) and DM-β-CyD were gifted from Nihon Shokuhin Kako (Tokyo, Japan). M-β-CyD (average degree of substitution = 10.5–14.7 per 7 glucose unit) was purchased from Sigma (St. Louis, MO). DM-α-CyD and TM-β-CyD were purchased from Wako Pure Chemical Industries (Osaka, Japan). Sulfobutyl ether β-CyD (SBE7-β-CyD) was gifted from CyDex (Lenexa, KS). F-12K culture medium, rhodamine 123 and propidium iodide (PI) were purchased from Invitrogen (Carlsbad, CA). Fetal calf serum (FCS) was obtained from JRH Biosciences (Renexa, KS). Hoechst 33342 and glutaraldehyde were obtained from Sigma (St. Louis, MO) and Nacalai Tesque (Kyoto, Japan), respectively. All other chemicals and solvents were of analytical reagent grade.

2.2. Preparation of macrophages

C57BL/6 mice (8–9 weeks old, wild type and p53$^{-/-}$) were injected with 1.0 ml of 3% thioglycollate intraperitoneally. On day 4, the peritoneal exude cells (PEC) were obtained by peritoneal lavage with 10 ml of ice-cold Hanks' balanced salt solution (HBSS, Ca^{2+} and Mg^{2+} free) supplemented with 10 U/ml of heparin. PEC were washed twice and resuspended in RPMI-1640 medium supplemented with 10% FCS, and overlaid on plastic culture plates. The plates were incubated in humidified 5% CO$_2$ for 2 h at 37 °C to allow macrophage adherence. Each plate was washed with gentle agitation by warmed RPMI-1640 to dislodge non-adherent cells, and a macrophage monolayer was obtained.

2.3. Cell viability

Cell viability was assayed by the WST-1 method (a Cell Counting Kit, Wako Pure Chemical Industries, Osaka, Japan), as reported previously (Hamasaki et al., 1996; Ono et al., 2001). Briefly, NR8383 cells, A549 cells and Jurkat cells were seeded at 5 × 10^4 cells onto

96-well microplate (Iwaki, Tokyo, Japan) and incubated for 2 h in a humidified atmosphere of 5% CO_2 and 95% air at 37 °C. Cells were washed twice with phosphate-buffered saline (PBS, pH 6.5), and then incubated for 1 h with 150 μL of F-12K culture medium supplemented with 15% FCS containing CyDs or Tween 20 at various concentrations in a humidified atmosphere of 5% CO_2 and 95% air at 37 °C. After washing twice with PBS to remove CyDs, 100 μL of fresh HBSS (pH 7.4) and 10 μL of WST-1 reagent were added to the plates and incubated for 1 h at 37 °C. The absorbance at 450 nm against a reference wavelength of 630 nm was measured with a miniplate reader (Nalge Nunc International NJ-2300, Rochester, NY).

2.4. Flow cytometry analysis

For determination of DNA content in cells, NR8383 cells (4×10^5) on 24-well culture plate (Iwaki, Tokyo, Japan) were incubated with culture medium containing CyDs for 24 h. After washing with PBS, cells were suspended and fixed with 100 μL of ice-cold 70% (v/v) ethanol for 3 h. After washing with PBS and subsequent centrifugation, cells were re-suspended with RNase A (100 μg/ml) and incubated for 30 min at 37 °C. After centrifugation, cells were re-suspended in a solution containing 100 μL of PI (20 μg/ml) and incubated for 20 min on ice before quantification using a FACSCalibur flow cytometer with CellQuest software (Becton Dickinson, Mountain View, CA).

Translocation of phosphatidylserine (PS) was detected by Tacs™ AnnexinV-FITC Apoptosis Detection Kits (R&D Systems, MN). NR8383 cells (1×10^5) and murine peritoneal macrophages obtained from wild type and $p53^{-/-}$ C57BL/6 mice (1×10^5) on 35-mm dish (Iwaki, Tokyo, Japan) were incubated with 5 mM CyDs containing culture medium for 24 h. After washed by PBS, the cells were stained with annexinV-FITC and PI followed by flow cytometry analysis as described above.

To measure the mitochondrial transmembrane potential $(\Delta\psi_m)$, rhodamine 123 was used as reported previously (Emaus et al., 1986). NR8383 cells (1×10^6) on 60-mm dish (Iwaki, Tokyo, Japan) were incubated with culture medium containing 5 mM CyDs for 24 h. After washed with PBS, cells were stained by rhodamine 123 (10 μM) for 15 min at 37 °C. Then, $\Delta\psi_m$ was analyzed by a FACSCalibur flow cytometer as described above.

2.5. DNA fragmentation assay

NR8383 cells $(1 \times 10^5/35$-mm dish) were incubated with culture medium containing 5 mM CyDs for 24 h. After washed with PBS, lysis buffer (10 mM Tris–HCl (pH 8.0), 10 mM EDTA·4Na, 0.5% Triton X-100) was added to the cells, and then incubated with RNase A (400 μg/ml) for 30 min at 37 °C. Furthermore, the cells were incubated with proteinase K (final concentration: 400 μg/ml) for 1 h at 50 °C. Gel electrophoresis was carried out at room temperature in TBE buffer (45 mM Tris–borate, 1 mM EDTA, pH8.0) in 2% agarose gel containing ethidium bromide (0.1 μg/ml) using Mupid™ system (Cosmo Bio, Tokyo, Japan) at 100 V for 40 min. The fragment DNA bands were visualized using an UV illuminator.

2.6. Determination of chromatin condensation

NR8383 cells were cultured in a glass-based 30 mm dish. After washed twice with PBS, the cells were incubated with 5 mM CyDs in culture medium for 24 h at 37 °C. After washed with PBS, the cells were fixed with 4% glutaraldehyde for 40 min. After incubation with 10 μg/ml of Hoechst 33342 in PBS for 10 min at 37 °C, the cells were scanned using the confocal fluorescence microscopic system (Olympus FV300-BX, Tokyo, Japan).
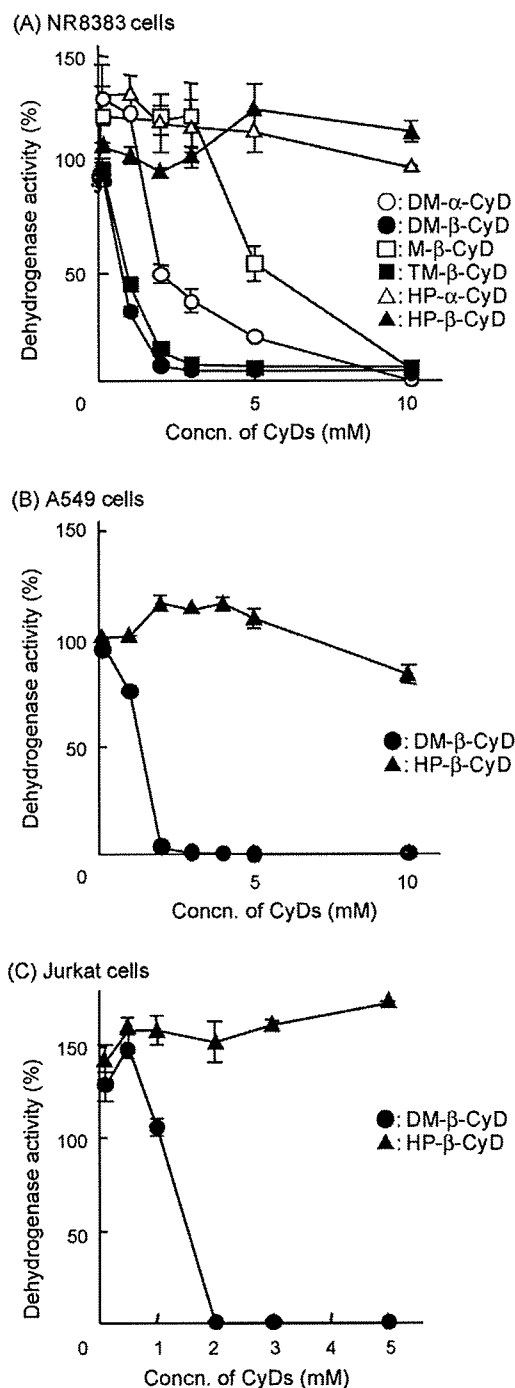

Fig. 1. Cytotoxicity of CyDs in NR8383 cells (A), A549 cells (B) and Jurkat cells (C). Cells were incubated with medium containing CyDs (0–10 mM) at 37 °C for 24 h. After washing twice with HBSS, cell viability was assayed by the WST-1 method. Each point represents the mean ± S.E.M. of three experiments.

2.7. Determination of phospholipids and cholesterol in supernatant

After NR8383 cells $(1 \times 10^5/35$-mm dish) were incubated with CyDs in HBSS at 37 °C for 1 h, the cell suspension was centrifuged at 10,000 rpm for 10 min. Total phospholipids in supernatant were determined using a Phospholipids-test Wako® (Wako Pure Chemical Industries, Osaka, Japan). For the cholesterol determination, the resulting supernatant (0.5 ml) was mixed with 1 ml of chloroform/methanol (15:2, v/v). After shaking for 10 min, the
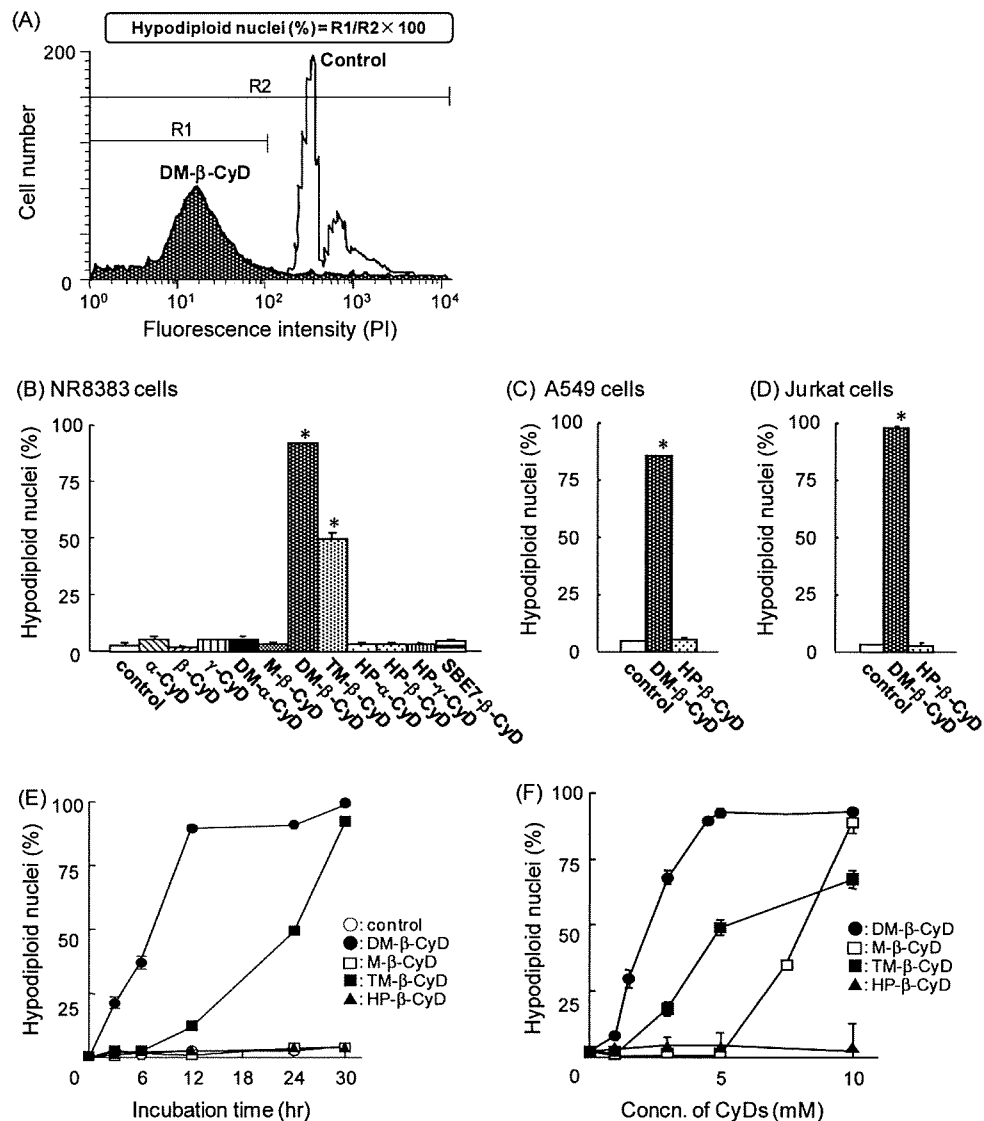
573

Fig. 2. Flow cytometric analysis of DNA content in NR8383 cells (A and B), A549 cells (C) and Jurkat cells (D) after treatment with 5 mM CyDs. Effects of incubation time of CyDs (E) and CyD-concentration (F) on DNA content in NR8383 cells. After incubation with CyDs for 24 h at 37 °C, the cells were stained by PI, and the percentage of cells showing DNA degradation was quantified by flow cytometry. Each value represents the mean ± S.E.M. of three experiments. *$p < 0.05$ versus control.

phase of chloroform was recovered and evaporated to concentrate membrane components. The concentrations of cholesterol in supernatants were determined using a Cholesterol-test Wako® (Wako Pure Chemical Industries, Osaka, Japan).

2.8. Western blot analysis

Akt, phospho-Akt, Bad, phospho-Bad, cytochrome c, and cytochrome oxidase IV in NR8383 cells were detected by Western blot analysis as reported previously (Li et al., 2006). Briefly, NR8383 cells (5×10^6 cells/60-mm dish) were incubated with 5 mM CyDs for 24 h. After washing with PBS, cells were lysed with 4× sample buffer (8% SDS, 40% glycerol, 24% β-mercaptoethanol in Tris–HCl buffer (pH 6.8)) and boiled for 5 min. After determining protein concentrations using the bicinchoninic acid reagent from Pierce Chemical (Rockford, IL), samples (20 μg as proteins) were separated with 10% (for the assay of Akt, phosphor-Akt and actin) and 15% (for the assay of Bad, phosphor-Bad, cytochrome c and cytochrome oxidase IV) SDS-PAGE and transferred onto Immobilon P membranes (Nihon Millipore, Tokyo, Japan). The membranes

were blocked with 5% skim milk in PBS containing 0.1% Tween 20 (PBS-T) and incubated with primary antibody (rabbit anti-Akt antibody), mouse anti-phospho-Akt antibody (Cell Signaling, Beverly, MA), mouse anti-Bad antibody, rabbit anti-phospho-Bad antibody, rabbit anti-actin antibody, rabbit anti-caspase-3 antibody (Santa Cruz, DE, CA), mouse anti-cytochrome c antibody and mouse anti-cytochrome oxidase subunit IV antibody (BD Pharmingen, Franklin, NJ) at 4 °C for overnight. After washing with PBS-T, the membranes were incubated with secondary antibody of peroxidase-conjugated sheep anti-mouse IgG antibody or peroxidase-conjugated donkey anti-rabbit IgG antibody (Amersham-pharmacia Biotech, Buckinghamshire, UK). Specific bands were detected using an ECL Western blotting analysis kit (Amersham Bioscience, Tokyo, Japan). The bands were detected using the Lumino-image analyzer LAS-1000 plus (Fujifilm, Tokyo, Japan).

2.9. Statistical analysis

Data are given as the mean ± S.E.M. Statistical significance of means for the studies was determined by analysis of variance

followed by Scheffe's test. *p*-Values for significance were set at 0.05.

3. Results

3.1. DM-β-CyD and TM-β-CyD induced apoptosis in NR8383 cells

The extent of cytotoxic activity of CyDs depends on the concentration of CyDs and the type of cells. Firstly, we examined cell viability in various cells after incubation with CyDs using by the WST-1 method. HP-α-CyD or HP-β-CyD did not decrease cell viability to NR8383 cells up to 10 mM after 24 h incubation (Fig. 1A). On the other hand, methylated CyD derivatives markedly reduced the viability of the cells in the order of M-β-CyD < DM-α-CyD < TM-β-CyD < DM-β-CyD. In addition, the strong cytotoxic activity of DM-β-CyD, not HP-β-CyD, in A549 cells and Jurkat cells was also observed (Fig. 1B and C). Thus, methylated CyDs strongly interact with various cells, compared to HP-CyDs.

To investigate whether methylated CyDs-induced cell death is accompanied by apoptotic feature, we next examined both the DNA content in nucleus and chromosomal DNA fragmentation using a flow cytometry and an agarose gel electrophoresis, respectively. Actually, the DNA content in nucleus was detected by the addition of PI through the intercalation into double strand DNA calculated as hypodiploid nuclei (%). The DNA content in nucleus after incubation with 5 mM DM-β-CyD for 24 h was strikingly decreased, compared to that in control (without CyD) in NR8383 cells (Fig. 2A). Fig. 2B shows the effects of CyDs on the DNA content in nucleus after incubation with various CyDs (5 mM) for 24 h in NR8383 cells. Of methylated CyDs, DM-β-CyD and TM-β-CyD, not DM-α-CyD or M-β-CyD, strikingly lowered the DNA content in the nucleus of the cells under the experimental conditions where complete cell death occurred (Figs. 1A and 2B). The DNA contents in nucleus in both A549 cells and Jurkat cells were also decreased by the treatment with DM-β-CyD (Fig. 2C and D). The decreasing DNA content by the treatment with DM-β-CyD or TM-β-CyD was incubation time-dependent and concentration-dependent (Fig. 2E and F). Meanwhile, no significant decrease in the DNA content was observed in natural CyDs, M-β-CyD, hydroxypropylated CyDs or SBE7-β-CyD in NR8383 cells (Fig. 2B), suggesting the safety profiles of these CyDs, consistent with previous findings of these CyDs (Irie and Uekama, 1997; Rajewski et al., 1995). Interestingly, DM-α-CyD did not change the DNA content even under the experimental condition where 80% of cell death was inducted (Fig. 2B). As shown in Fig. 3, the agarose gel electrophoresis study revealed that DNA fragmentation in NR8383 cells occurred after incubation with DM-β-CyD or TM-β-CyD. Additionally, DNA fragmentation caused by DM-β-CyD was incubation time-dependent and concentration-dependent (Fig. 3B and C).

Next, we observed the morphological changes in NR8383 cells after incubation with β-CyDs for 24 h using a fluorescence microscopy. To visualize the chromatin condensation in cells, Hoechst 33342 was used as a DNA-binding fluorescence dye. Condensed and segmented nuclei were observed in the cells treated with DM-β-CyD and TM-β-CyD, but neither M-β-CyD nor HP-β-CyD (Fig. 4). These results are well consistent with the results of DNA content analysis and DNA fragmentation analysis (Figs. 2 and 3). These findings suggest that DM-β-CyD and TM-β-CyD induce apoptosis in NR8383 cells.

3.2. Effects of methylated CyDs on PS externalization

A critical event during apoptosis appears to be the acquisition of plasma membrane changes that allows phagocytes to recog-
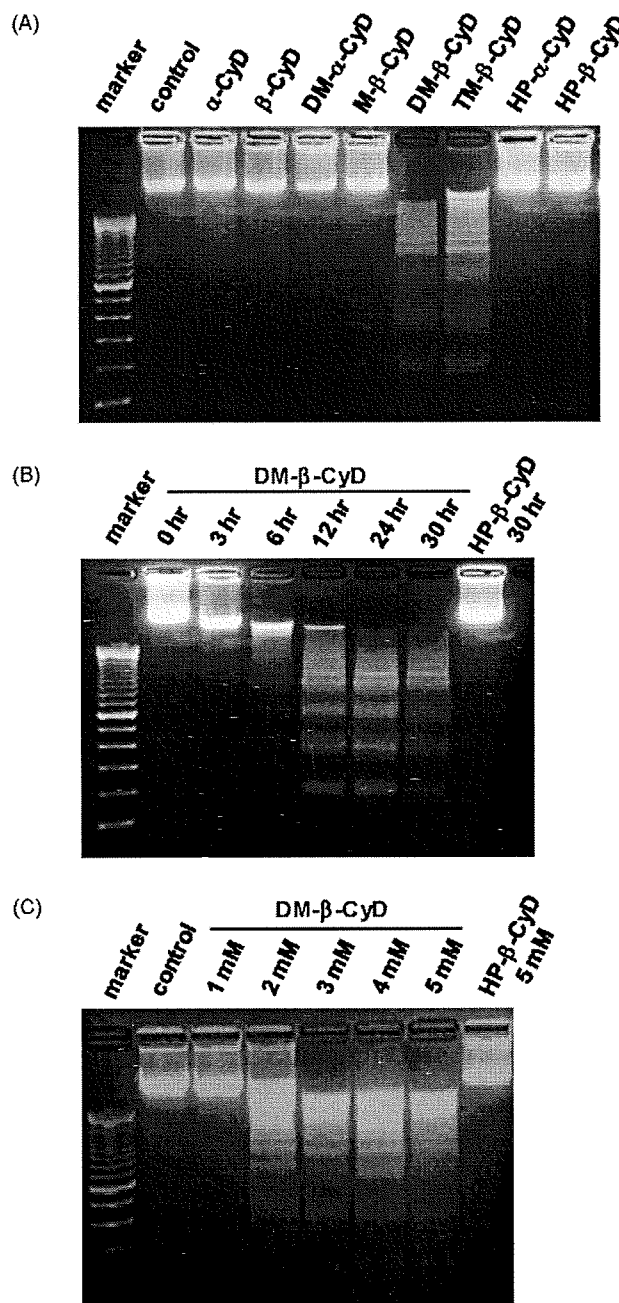
(A)

(B)

(C)

Fig. 3. (A) Agarose gel electrophoresis of DNA extracted from NR8383 cells treated with CyDs. Time-dependent effect (B) and concentration-dependent effect (C) of CyDs on apoptosis in NR8383 cells were shown. NR8383 cells were incubated with medium containing CyDs at 1 mM for 24 h at 37 °C. After incubation, cells were lysed and then analyzed DNA fragmentation using a gel electrophoresis.

nize and engulf these cells before they rupture. Then, we next examined the effects of methylated CyDs on PS externalization in early apoptotic cells. The treatment of NR8383 cells with 5 mM DM-β-CyD or TM-β-CyD for 24 h significantly increased in the number of annexinV-FITC(+)/PI(−) cells as early apoptosis (Fig. 5A and B), however, the treatment with 5 mM DM-α-CyD, HP-β-CyD or M-β-CyD did not increase them, although cell death occurred under the present experimental conditions (Fig. 1A). In addition, we confirmed that the extent of PS externalization after treatment with DM-β-CyD increased in a time-dependent manner (data not shown). These results strongly suggest that cell death induced by DM-β-CyD and TM-β-CyD results from apoptosis.
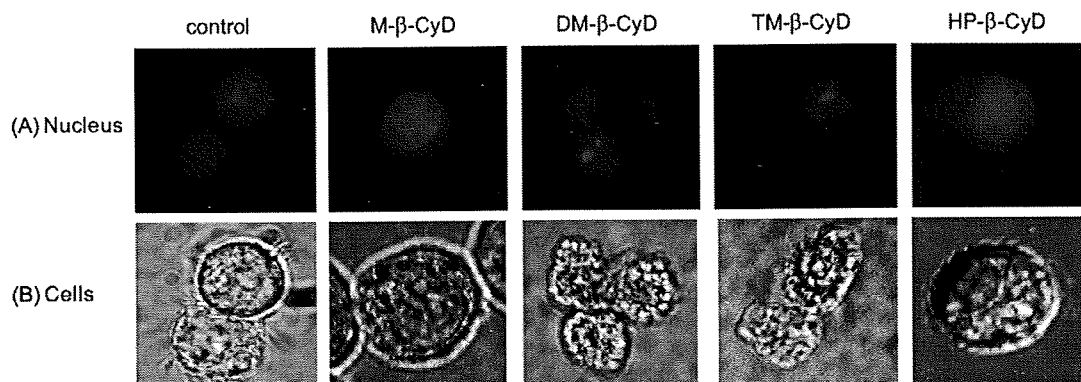
Fig. 4. Fluorescence (A) and phase contrast (B) micrographs of NR8383 cells treated with β-CyDs. After incubation with medium containing β-CyDs (5 mM) for 24 h at 37 °C, NR8383 cells were stained by Hoechst 33342, and condensations of chromatin were detected using a fluorescence microscope.

3.3. Membrane lipids such as cholesterol and phospholipids released by CyDs

Lipid rafts are mainly composed of cholesterol and sphingolipids such as sphingomyelin in the cell membranes, and contain various signal transduction molecules including growth factor receptors (Le Roy and Wrana, 2005). We previously reported that CyDs showed hemolytic activity at high concentrations through the extraction of cell membrane components such as cholesterol and phospholipids in cell membranes (Ohtani et al., 1989; Irie and Uekama, 1997). Recently, we reported that DM-β-CyD induced morphological change of RRBC to echinocyte through the extraction of cholesterol from cholesterol-rich lipid rafts (Motoyama et al., 2009), while DM-α-CyD induced morphological changes to stomatocyte by the extraction of sphingomyelin from sphingolipid-rich lipid rafts, but not extraction of cholesterol (Motoyama et al., 2009). Therefore, to gain insight into the mechanism of apoptosis induced by DM-β-CyD and TM-β-CyD, we investigated that the effects of CyDs on the release of cholesterol and phospholipids from NR8383 cells. Cholesterol and phospholipids released in supernatant after incubation with 5 mM CyDs for 1 h were determined by Cholesterol-test Wako® and Phospholipids-test Wako®, respectively. The extent of cholesterol released from NR8383 cells by treated with β-CyDs was increased in the order of DM-α-CyD ≪ HP-β-CyD < M-β-CyD < TM-β-CyD < DM-β-CyD (Fig. 6A). Meanwhile, DM-α-CyD and DM-β-CyD remarkably released phospholipids in the supernatant, but the others did not (Fig. 6B). These results suggest that DM-β-CyD and TM-β-CyD induced apoptosis through the cholesterol depletion in cell membranes. Next, we examined whether apoptosis induced by the treatment with DM-β-CyD is suppressed by the addition of cholesterol in culture medium using a flow cytometry. As shown in Fig. 6C, apoptosis induced by DM-β-CyD in NR8383 cells was significantly suppressed by the addition of cholesterol. These results suggest that DM-β-CyD induces apoptosis through cholesterol depletion from cell membranes.

3.4. DM-β-CyD induced apoptosis in NR8383 cells via PI3K-Akt-Bad pathway

It is well known that Akt kinase activity is induced following PI3K activation in various growth factor receptor-mediated signaling cascades (Franke et al., 2003). On the other hand, p38 MAPK is stress-activated protein kinase and has an important role in apoptotic signal transduction (Davis, 2000). Therefore, we next investigated the effects of DM-β-CyD on PI3K-Akt and MAPK pathways. Hereafter, we employed HP-β-CyD as a negative control because of the lack of apoptotic activity under the experimen-

tal conditions. Apoptosis induced by DM-β-CyD was significantly increased by the pretreatment of NR8383 cells with LY294002, a PI3K specific inhibitor (Fig. 7A). However, no significant change was observed in pretreatment with SB203580, a p38 MAP kinase inhibitor in NR8383 cells (Fig. 7B). These results suggest that apoptosis induced by DM-β-CyD is involved in PI3K rather than p38 MAP kinase. Next, we investigated the effects of DM-β-CyD on Akt activation. Then, Akt and its activating form (phospho-Akt) were determined by Western blot analysis using an anti-Akt antibody and anti-phospho-Akt antibody, respectively. As shown in Fig. 7C, the bands corresponding to Akt and phospho-Akt in NR8383 cells after incubation with 5 mM DM-β-CyD for 24 h were markedly down-regulated, compared with those of control and HP-β-CyD. In addition, DM-β-CyD down-regulated Akt in NR8383 cells as the incubation time with DM-β-CyD increased (Fig. 7D). Furthermore, phosphorylation of Bad, an apoptosis inducible Bcl-2 family protein, was also ameliorated by the treatment with DM-β-CyD (Fig. 7E). These results strongly suggest that DM-β-CyD induces apoptosis through the impairment of activation of PI3K-Akt pathway, not p38 MAPK, followed by the inhibition of phosphorylation of Bad.

3.5. Effects of DM-β-CyD on p53 pathway

The tumor suppressor activity of the p53 protein has been explained by its ability to induce apoptosis in response to a variety of cellular stresses (Fridman and Lowe, 2003). Recent studies have demonstrated that p53 interacts with the pro-apoptotic mitochondrial membrane protein Bak in the induction of apoptosis (Leu et al., 2004). Therefore, to reveal whether p53 is involved in the apoptosis induced by DM-β-CyD, we examined the apoptotic activity of DM-β-CyD in mouse peritoneal macrophages isolated from wild type mice or p53 knockout (p53$^{-/-}$) mice using a flow cytometry after treatment with annexinV-FITC. As shown in Fig. 8, there was no significant difference in the amount of apoptotic cells of peritoneal macrophages between wild type and p53$^{-/-}$ mice. These results suggest that the involvement of p53 in apoptosis induced by DM-β-CyD was only slight.

3.6. Involvement of mitochondria in apoptosis induced by DM-β-CyD

To reveal whether the apoptotic effect of DM-β-CyD is mitochondria-dependent or not, we determined the mitochondrial transmembrane potential using rhodamine 123 after incubation with DM-β-CyD in NR8383 cells (Emaus et al., 1986). The mitochondrial transmembrane potentials of the cells treated with
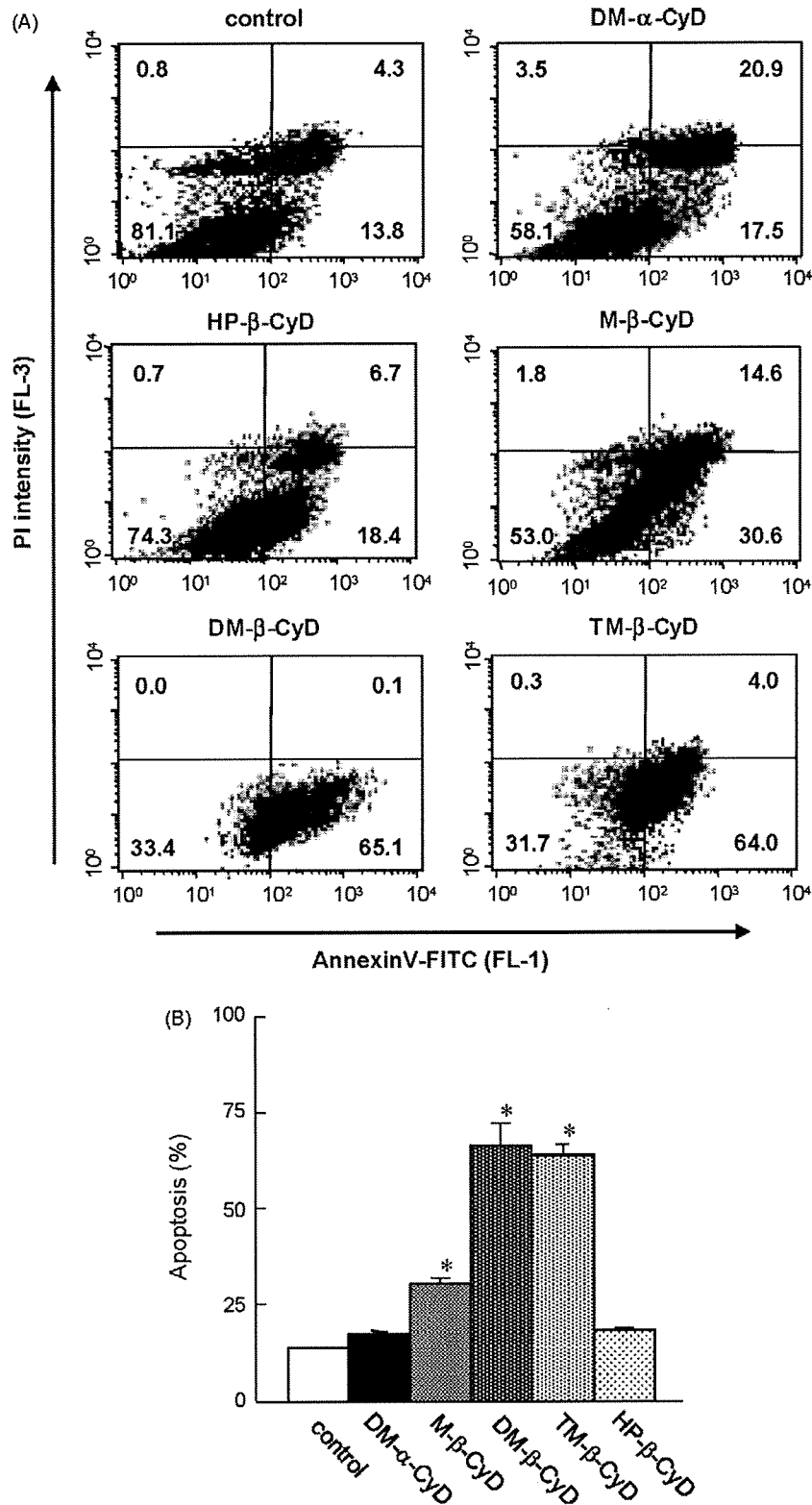
Fig. 5. Effects of CyDs on exposure of PS in NR8383 cells. NR8383 cells were incubated in medium with or without CyDs (5 mM) for 24 h. Then cells were stained with annexinV-FITC and PI, and analyzed using a flow cytometry. (A) Data were plotted as the annexinV-FITC intensity (X-axis) versus the relative number of PI-positive cells (Y-axis). (B) The percentage of cells existing in annexinV-FITC-positive and PI-negative fraction was shown. Each value represents the mean ± S.E.M. of three experiments. *p < 0.05 versus control.
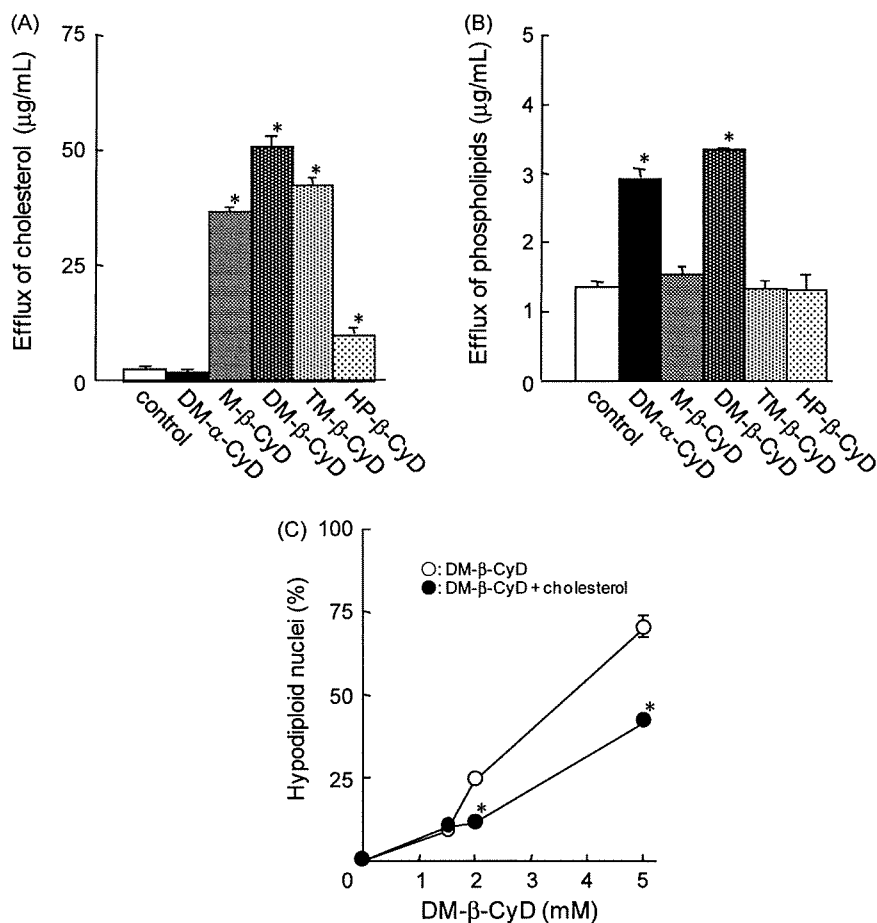
Fig. 6. Effects of CyDs on efflux of cholesterol (A) and phospholipids (B) from NR8383 cells. (A and B) NR8383 cells were incubated in HBSS (pH 7.4) with or without CyDs (5 mM) for 1 h. The concentrations of cholesterol and phospholipids in HBSS were determined by Cholesterol E-test Wako® and Phospholipids C-test Wako®, respectively. Each value represents the mean ± S.E.M. of three experiments. $*p < 0.05$ versus control. (C) Effects of cholesterol on apoptosis induced by DM-β-CyD. NR8383 cells were treated with 5 mM DM-β-CyD or cholesterol-loading 5 mM DM-β-CyD for 24 h at 37 °C. After treatment, cells were stained by PI, then the percentage of cells showing DNA degradation was quantified by flow cytometry. Each point represents the mean ± S.E.M. of three experiments. $*p < 0.05$ versus DM-β-CyD.

DM-β-CyD and TM-β-CyD were significantly lowered to 1% and 16%, respectively, but those with DM-α-CyD, HP-β-CyD and M-β-CyD decreased to 56%, 87% and 56%, respectively (Fig. 9A and B). It is acknowledged that a decrease in mitochondrial potential leads to the release of cytochrome c from mitochondria followed by activation of caspase-9 and caspase-3 through the formation of apoptosome (Wang, 2001). Therefore, we determined the release of cytochrome c from mitochondria after treatment with DM-β-CyD according to the method reported previously (Yang et al., 1997). Successful separation of mitochondrial fractions was validated by determination of cytochrome oxidase IV, a mitochondrial electron transport protein. As shown in Fig. 9C, the only faint band corresponding to cytochrome c in mitochondrial fractions of NR8383 cells after treatment with DM-β-CyD was observed, probably due to the release of cytochrome c from mitochondria. These results suggest that the apoptosis induced by DM-β-CyD is associated with a mitochondria-dependent pathway.

3.7. Activation of caspase-3 by DM-β-CyD

Caspase cleaves itself or other caspase to convert inactive form (pro-caspase) to active form, and degrade the substrate such as ICAD, PARP (poly(ADP-ribose) polymerase), and actin. Cytochrome c is found to activate caspase-9 through binding with Apaf-1, ATP, and pro-casepase-9, results in the activation of caspase-3 (Kroemer

and Reed, 2000; Wang, 2001). Therefore, we next examined the effects of DM-β-CyD on caspase-3 activation by Western blot analysis. Treatment of NR8383 cells with DM-β-CyD, not HP-β-CyD, for 24 h, cleaved pro-caspase-3, and then activated caspase-3 (Fig. 10A). Furthermore, the band intensity of actin, one of substrate of capase-3, was decreased by the treatment with DM-β-CyD, not HP-β-CyD, in a time-dependent manner (Fig. 10B). These results suggest that DM-β-CyD induces apoptosis through the activation of caspase-3, resulting from release of cytochrome c from mitochondria.

4. Discussion

In the present study, we revealed that of various CyDs, DM-β-CyD potentially caused apoptosis in NR8383, A549 and Jurkat cells, possibly due to cholesterol depletion from cell membranes, and apoptosis induced by DM-β-CyD could result from the inhibition of the activation of PI3K-Akt-Bad pathway, neither p38 MAP kinase nor p53.

Cytotoxicity induced by DM-β-CyD documented herein was found to induce loss of cell viability through apoptotic cell death. The apoptotic character of the cell death was confirmed by the DNA content in nucleus, DNA fragmentation, morphological change, mitochondrial transmembrane potential, cytochrome c release from mitochondria, and caspase-3 activation in NR8383 cells. As